

# 000 001 002 003 004 005 006 007 008 009 010 011 012 013 014 015 016 017 018 019 020 021 022 023 024 025 026 027 028 029 030 031 032 033 034 035 036 037 038 039 040 041 042 043 044 045 046 047 048 049 050 051 052 053 FEDERATED SKETCHING LoRA: A FLEXIBLE FRAME- WORK FOR HETEROGENEOUS COLLABORATIVE FINE- TUNING OF LLMs

Anonymous authors

Paper under double-blind review

## ABSTRACT

Fine-tuning large language models (LLMs) on resource-constrained clients remains a challenging problem. Recent works have fused low-rank adaptation (LoRA) techniques with federated fine-tuning to mitigate challenges associated with client model sizes and data scarcity. Still, the heterogeneity of resources remains a critical bottleneck: while higher-rank modules generally enhance performance, varying client capabilities constrain LoRA’s feasible rank range. Existing approaches attempting to resolve this issue either lack analytical justification or impose additional computational overhead, leaving a wide gap for efficient and theoretically-grounded solutions. To address these challenges, we propose federated sketching LoRA (FSLoRA), which leverages a sketching mechanism to enable clients to selectively update submatrices of global LoRA modules maintained by the server. By adjusting the sketching ratios, which determine the ranks of the submatrices on the clients, FSLoRA flexibly adapts to client-specific communication and computational constraints. We provide a rigorous convergence analysis of FSLoRA that characterizes how the sketching ratios affect the convergence rate. Through comprehensive experiments on multiple datasets and LLM models, we demonstrate FSLoRA’s performance improvements compared to various baselines.

## 1 INTRODUCTION

Lightweight client-side large language models (LLMs) have recently gained significant attention as a promising complement to cloud-based LLMs (Fan et al., 2024). They align with the typical paradigm of LLMs: starting from a base model pre-trained on large-scale datasets to learn general linguistic patterns, semantics, and context, and then undergoing fine-tuning on task-specific data to enhance performance on specialized or domain-specific applications. However, an LLM fine-tuned on a single client often achieves unsatisfactory performance due to the limited data. Federated learning (McMahan et al., 2017; Chen et al., 2023) has been investigated as a potential solution here, enabling the model to be fine-tuned across a group of distributed clients within the same task domain, without any raw data sharing.

However, federated LLM fine-tuning is costly in both computation and communication due to the massive parameter volume. Importantly, many parameter-efficient fine-tuning methods have been proposed (Lester et al., 2021; Li and Liang, 2021; Hu et al., 2021) to reduce the model adaptation cost. Among them, low-rank adaptation (LoRA) (Hu et al., 2021) stands out as a particularly effective approach due to its flexibility. In particular, LoRA enables efficient fine-tuning by approximating weight updates  $\Delta\mathbf{W}$  through a low-rank decomposition  $\Delta\mathbf{W} = \mathbf{B}\mathbf{A}$ , where matrices  $\mathbf{B}$  and  $\mathbf{A}$  contain significantly fewer trainable parameters than the original weight matrix. Building on this foundation, recent works have combined LoRA with federated averaging (FedAvg) (Zhang et al., 2024; Ye et al., 2024), showing that federated LoRA significantly reduce the training overhead.

**Challenges.** While incorporating LoRA into federated LLM fine-tuning reduces the number of trainable parameters, *computation and communication costs are still forced to increase with the LoRA rank*. This poses challenges when complex tasks demand higher-rank LoRA modules, particularly on resource-constrained clients. Furthermore, the *heterogeneity in resource availability across distributed clients makes a uniform rank adopted in federated LoRA inefficient*: a fixed rank  $r$  may be too large

for some constrained clients, while being too small for more powerful ones, resulting in underutilized resources. Consequently, an approach that further reduces computation and communication overhead while adapting LoRA ranks to heterogeneous client capabilities is highly desirable. Although some existing approaches have attempted to provide a solution (Cho et al., 2024; Bai et al., 2024; Wang et al., 2024), they either lack theoretical justification or impose additional computational overhead, leaving a gap for an efficient and theoretically-grounded solution. As we discuss in Section 2.2, a comprehensive approach that preserves the analytical and practical benefits of LoRA while enabling heterogeneous collaborative fine-tuning under tight resource constraints remains elusive.

## 1.1 CONTRIBUTIONS

Motivated by these limitations, this work develops a methodology for efficient federated LLM fine-tuning that (i) retains the flexibility of LoRA, (ii) provides theoretical convergence guarantees, and (iii) addresses the challenges posed by heterogeneous and constrained resources across distributed clients. As depicted in Figure 1, our key idea is to introduce a sketching-based LoRA update to the local fine-tuning, which allows clients to selectively update a subset of columns and rows of the LoRA modules during each round, reducing the computation and communication consumption. Additionally, our method customizes the fine-tuning process by adjusting the sparsity level of the sketching matrix, i.e., the size of the updated submatrices for each client in each iteration. As we will see, the impact of the introduced sketching mechanism on the overall optimization landscape requires careful modeling consideration, posing additional challenges for the theoretical analysis that we address in this work.

Overall, we make the following contributions:

- We propose federated sketching LoRA (FSLoRA), which leverages a sketching mechanism to enable clients to selectively update submatrices of global LoRA modules maintained by the server. By adjusting the sketching ratios, which determine the ranks of the submatrices on clients, FSLoRA effectively adapts to client-specific communication and computational constraints.
- We present a rigorous convergence analysis of FSLoRA under non-uniform submatrix update scenarios (i.e., heterogeneous LoRA configurations) across clients, revealing how the sketching ratios affect the convergence rate via scaled smoothness constants. Further, our results show that while increasing the sketching ratios improves convergence theoretically, it also raises communication and computation costs, suggesting a potential trade-off in selecting the sketching ratios.
- We conduct extensive experiments across multiple datasets and LLM models with diverse parameter settings, demonstrating FSLoRA’s superior performance compared to various baselines in accuracy, training time, and resource utilization. Our ablation studies further validate the effectiveness of the sketching mechanism and the ability of clients to exploit larger global ranks under FSLoRA.

## 1.2 RELATED WORKS

**Collaborative fine-tuning via federated LoRA:** Federated LoRA is an efficient approach for collaborative LLM fine-tuning among distributed clients (Chen et al., 2023; Sun et al., 2024; Guo et al., 2025). Building on this foundation, Kuo et al. (2024) proposed integrating communication compression with federated LoRA to further reduce communication overhead. Meanwhile, Bai et al. (2024); Cho et al. (2024); Byun and Lee (2024); Wang et al. (2024); Koo et al. (2024) explored the challenges of resource heterogeneity across distributed clients and introduced heterogeneous LoRA as a solution. However, the approaches proposed in (Cho et al., 2024; Koo et al., 2024; Byun and Lee,

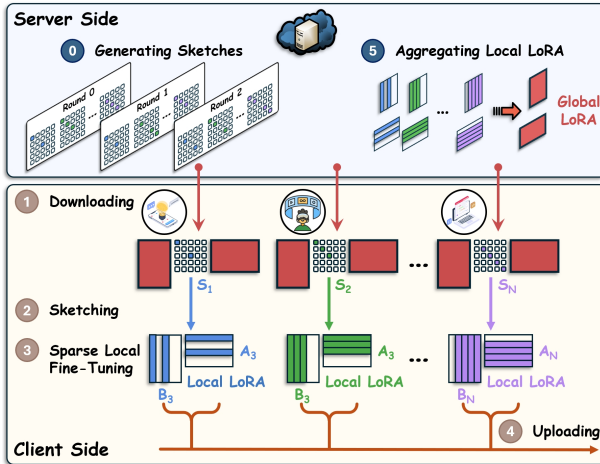


Figure 1: An illustration of our proposed methodology where the server maintains a pair of global LoRA modules while the clients adaptively update submatrices of the global LoRA modules through sketching during each round.

108 2024; Bai et al., 2024) lack a theoretical foundation. Moreover, the FlexLoRA method introduced  
 109 in (Bai et al., 2024) incurs additional computational overhead due to its reliance on singular value  
 110 decomposition (SVD). Furthermore, the FLoRA algorithm proposed in (Wang et al., 2024) requires  
 111 the clients to merge the LoRA modules into the base model, thereby compromising the inherent  
 112 flexibility of LoRA. Overall, there is still a lack of a systematic and theoretically grounded solution  
 113 that can effectively tackle heterogeneous collaborative LLM fine-tuning.

114 **Enhancing adaptability via higher-rank LoRA modules:** The foundational study by Hu et al.  
 115 (2021) demonstrated that small ranks can be sufficient for certain tasks; however, they also acknowl-  
 116 edge that small rank LoRA modules may not work universally, especially when the downstream task  
 117 differs significantly from pretraining. Following this, several works explored the effect of increasing  
 118 the rank in LoRA modules. In a centralized setup, Kalajdzievski (2023) and Shuttleworth et al. (2024)  
 119 showed that higher-rank LoRA models can closely approximate full fine-tuning under rsLoRA. In  
 120 a federated LLM fine-tuning regime, Bai et al. (2024) demonstrated improved performance with  
 121 larger ranks under FlexLoRA. Similarly, Cho et al. (2024) reported that, with proper overfitting  
 122 control, HeteroLoRA can also benefit from larger ranks. Overall, while small ranks may suffice for  
 123 simpler tasks or strong base models, higher-rank modules are necessary to compensate for limited  
 124 backbone capability, such as in lightweight LLMs, and to enable effective adaptation to more complex  
 125 downstream tasks.

126 **Sketching-based optimization:** Sketching is an efficient technique for mitigating the complexity of  
 127 high-dimensional optimization, with its earliest applications in least-squares regression (Sarlos, 2006;  
 128 Wang et al., 2022). Beyond this, gradient sketching has been employed to construct preconditioners  
 129 for gradient descent methods (Gower and Richtárik, 2015). Building on these foundations, recent  
 130 work has applied sketching to distributed optimization. In particular, Charalambides and Mazumdar  
 131 (2024) proposed hybrid local-global sketching for distributed least-squares, while Demidovich et al.  
 132 (2023) developed a distributed sparsified training framework based on sketching. Shrivastava et al.  
 133 (2024) demonstrated that sketching substantially reduces communication in distributed training of  
 134 overparameterized deep models without sacrificing accuracy. More recently, Nicolas et al. (2025)  
 135 investigated sketching-based differential privacy and demonstrated its compatibility with secure  
 136 aggregation. Despite these advances, sketching strategies tailored to structured low-rank adaptation  
 137 modules such as LoRA remain largely unexplored.

## 2 PROBLEM BACKGROUND

### 2.1 LORA-BASED FEDERATED LLM FINE-TUNING

141 The federated LoRA fine-tuning problem can be formulated as

$$142 \min_{\mathbf{B}, \mathbf{A}} f(\mathbf{B}, \mathbf{A}) := \frac{1}{N} \sum_{i=1}^N f_i(\mathbf{B}, \mathbf{A}), \text{ where } f_i(\mathbf{B}, \mathbf{A}) := \mathbb{E}_{\xi \sim \mathcal{D}_i} [\ell(\mathbf{W}_0 + \mathbf{B}\mathbf{A}, \xi)], \quad (1)$$

145 where  $\mathbf{W}_0$  denotes the frozen base model,  $\mathbf{B} \in \mathbb{R}^{m \times r}$ ,  $\mathbf{A} \in \mathbb{R}^{r \times n}$  are LoRA modules,  $N$  denotes  
 146 the number of clients,  $\xi$  denotes a data sample, and  $\mathcal{D}_i$  is the local dataset on client  $i$ .  $\ell$ ,  $f_i$ , and  $f$  are  
 147 the sample loss function, the local loss for client  $i$ , and the global loss, respectively.

148 Problem (1) aligns with the conventional federated optimization formulation, which thus can be  
 149 solved using the FedAvg algorithm. Based on the FedAvg framework, Zhang et al. (2024) developed  
 150 federated LoRA, which applies a uniform rank  $r$  across all clients, overlooking resource heterogeneity.  
 151 This one-size-fits-all approach leads to resource mismatches, where computationally constrained  
 152 clients may struggle, while more powerful clients remain underutilized with a fixed rank.

### 2.2 AREN'T THE EXISTING SOLUTIONS GOOD ENOUGH?

154 To address this issue, researchers have proposed heterogeneous federated LoRA approaches, where  
 155 clients maintain non-uniform LoRA modules with varying ranks. They also introduce mechanisms to  
 156 overcome the challenges of directly aggregating matrices with different dimensions. However, these  
 157 methods often lack theoretical foundation or incur additional computational and memory overhead.

158 **HeteroLoRA (Cho et al., 2024)** lets the server pad the updates from the clients with smaller ranks to  
 159 match the size of the largest rank during aggregation. During model dissemination, clients receive  
 160 a truncated version of the global LoRA modules from the server. Although easy to implement,

162 HeteroLoRA is primarily heuristic in nature and lacks a rigorous theoretical foundation, potentially  
 163 limiting its performance, as we will see in Section 5.

164 **FlexLoRA (Bai et al., 2024)** requires the server to collect the individual LoRA matrices  $\mathbf{B}_i$  and  $\mathbf{A}_i$   
 165 from the clients and then computes their product  $\mathbf{B}_i \mathbf{A}_i$ . To support the initialization of non-uniform  
 166 LoRA modules, the server applies truncated SVD to the averaged product  $\frac{1}{N} \sum_{i=1}^N \mathbf{B}_i \mathbf{A}_i$ . However,  
 167 this approach introduces extra computational and memory overhead on the server due to truncated  
 168 SVD, and the associated error can limit the performance as demonstrated in Section 5.  
 169

170 **FLoRA (Wang et al., 2024)** introduces a stacking mechanism where the server concatenates LoRA  
 171 modules from the clients. The concatenated matrices are then sent back to the clients, which compute  
 172 their product and merge it into the base model before initializing new LoRA modules for the next  
 173 fine-tuning round. However, this approach increases communication complexity linearly with the  
 174 number of clients, imposes higher computation and memory demands on the clients, and compromises  
 175 LoRA’s flexibility to support multiple adapters for different tasks.  
 176

177 More detailed comparisons on computation, memory, and communication are presented in Appendix  
 178 A. In summary, a theoretically-grounded solution that preserves LoRA’s benefits while effectively  
 179 addressing resource heterogeneity across distributed clients remains lacking.

### 3 FEDERATED SKETCHING LORA

181 Motivated by the limitations of existing methods, we propose a new federated LoRA reformulation.  
 182 Building on this foundation, we develop FSLoRA, a heterogeneous LoRA algorithm that preserves  
 183 LoRA’s flexibility while accommodating client resource heterogeneity.  
 184

#### 3.1 OUR FORMULATION

185 We propose a sketching-based LoRA formulation for collaborative LLM fine-tuning as follows:  
 186

$$187 \min_{\mathbf{B}, \mathbf{A}} f^S(\mathbf{B}, \mathbf{A}) := \frac{1}{N} \sum_{i=1}^N f_i^S(\mathbf{B}, \mathbf{A}) \text{ where } f_i^S(\mathbf{B}, \mathbf{A}) := \mathbb{E}_{\mathbf{S} \sim \mathcal{S}_i; \xi \sim \mathcal{D}_i} [\ell(\mathbf{W}_0 + \mathbf{BSA}, \xi)], \quad (2)$$

188 where  $\mathbf{B} \in \mathbb{R}^{m \times r}$ ,  $\mathbf{A} \in \mathbb{R}^{r \times n}$  are LoRA modules,  $f_i^S$  is the local loss function at client  $i$  with  
 189 sketching, and  $\mathbf{S}$  denotes a sketching matrix randomly sampled from the diagonal matrix set  $\mathcal{S}_i =$   
 190  $\mathcal{S}(r, k_i)$ . The set  $\mathcal{S}(r, k_i)$  comprises diagonal matrices of size  $r \times r$  with exactly  $k_i$  non-zero entries.  
 191 The formal definition of  $\mathcal{S}(r, k)$  is provided below:  
 192

193 **Definition 3.1** (Random- $k$  sketching). A random- $k$  diagonal matrix set is defined as:  
 194

$$195 \mathcal{S}(r, k) = \left\{ \mathbf{S} \mid \mathbf{S} = \frac{r}{k} \sum_{j \in \mathcal{I}} \mathbf{e}_j \mathbf{e}_j^\top, \mathcal{I} \subseteq \{1, \dots, r\}, |\mathcal{I}| = k \right\}, \quad (3)$$

196 where  $\mathbf{e}_1, \dots, \mathbf{e}_r \in \mathbb{R}^r$  are standard unit basis vectors and index set  $\mathcal{I}$  is a random subset of  
 197  $[r] := \{1, 2, \dots, r\}$  sampled uniformly from all subsets of  $[r]$  with cardinality  $k$ .  
 198

199 With  $\mathbf{S}$  being a matrix sampled from  $\mathcal{S}_i$ , we have  $\mathbf{BSA} = \frac{r}{k_i} \sum_{j \in \mathcal{I}_i} \mathbf{B} \mathbf{e}_j \mathbf{e}_j^\top \mathbf{A}$ , where  $\mathcal{I}_i$  corresponds  
 200 to the index set of non-zero diagonal entries of  $\mathbf{S}$ .  $\mathbf{B} \mathbf{e}_j$  extracts the  $j$ -th column of  $\mathbf{B}$  while  $\mathbf{e}_j^\top \mathbf{A}$   
 201 extracts the  $j$ -th row of  $\mathbf{A}$ . In other words, only  $k_i$  columns and rows in the LoRA modules  $\mathbf{B}$  and  $\mathbf{A}$   
 202 are activated by the sketching matrix in the loss  $\ell(\mathbf{W}_0 + \mathbf{BSA}, \xi)$  at client  $i$ . On the other hand, the  
 203 sketching matrix  $\mathbf{S}$  satisfies  $\mathbb{E}_{\mathbf{S} \sim \mathcal{S}_i} [\mathbf{S}] = \mathbf{I}_r$  where  $\mathbf{I}_r$  is a  $r$ -dimensional identity matrix. Based upon  
 204 this property,  $\mathbf{W}_0 + \mathbf{BSA}$  can be treated as an unbiased estimate of  $\mathbf{W}_0 + \mathbf{BA}$ .  
 205

206 **Intuition:** A larger rank allows LoRA modules to be more expressive, leading to better performance  
 207 (Bai et al., 2024; Kalajdzievski, 2023; Shuttleworth et al., 2024). However, resource-constrained  
 208 clients cannot afford the computational or communication demands of large-rank modules. Our  
 209 formulation (2) leverages the sketching matrix to balance the expressiveness of high-rank LoRA  
 210 modules with the resource constraints of different clients. With the sketching mechanism introduced,  
 211 the local gradients with respect to the LoRA modules on the clients will exhibit structured sparsity. By  
 212 adjusting the sketching ratio  $k_i/r$ , we can tailor the sparsity of the gradient to match the capabilities  
 213 of each client, ensuring affordable training while maintaining performance across heterogeneous  
 214 systems, as elaborated in the following subsection. Overall, compared to (1), our formulation offers a  
 215 more flexible framework, tailored to address the diverse capabilities of heterogeneous clients.

216 3.2 SPARSITY IN THE GRADIENTS  
217

218 In this subsection, we analyze the gradient structure of LoRA modules and highlight the gradients' 219 sparsity properties under a given sketching matrix. To begin, we present the gradient expressions for 220 the LoRA modules  $\mathbf{B}$  and  $\mathbf{A}$  in the following lemma. The proof is provided in Appendix J.2.

221 **Lemma 3.2** (Gradient Formulation). *For a given sketching matrix  $\mathbf{S}$ , the gradients of  $\ell(\mathbf{W}_0 +$  222  $\mathbf{BSA}, \xi)$  with respect to  $\mathbf{B}$  and  $\mathbf{A}$  take the following form*

$$\begin{aligned} \nabla_{\mathbf{B}} \ell(\mathbf{W}_0 + \mathbf{BSA}, \xi) &= \nabla \ell(\mathbf{W}_0 + \mathbf{BSA}, \xi) \mathbf{A}^\top \mathbf{S}^\top \\ \nabla_{\mathbf{A}} \ell(\mathbf{W}_0 + \mathbf{BSA}, \xi) &= \mathbf{S}^\top \mathbf{B}^\top \nabla \ell(\mathbf{W}_0 + \mathbf{BSA}, \xi), \end{aligned} \quad (4)$$

226 where  $\nabla_{\mathbf{B}} \ell(\mathbf{W}_0 + \mathbf{BSA}, \xi)$ ,  $\nabla_{\mathbf{A}} \ell(\mathbf{W}_0 + \mathbf{BSA}, \xi)$ , and  $\nabla \ell(\mathbf{W}_0 + \mathbf{BSA}, \xi)$  represent the gradients 227 of  $\ell(\mathbf{W}_0 + \mathbf{BSA}, \xi)$  with respect to  $\mathbf{B}$ ,  $\mathbf{A}$ , and  $\mathbf{W}_0 + \mathbf{BSA}$ , respectively.

229 In particular, a random- $k$  diagonal sketching matrix selectively samples  $k$  rows or columns of a matrix 230 through left product or right product, respectively. With  $\mathbf{S}$  being a random- $k$  diagonal matrix, the 231 gradients of  $\ell(\mathbf{W}_0 + \mathbf{BSA}, \xi)$  with respect to LoRA modules  $\mathbf{B}$  and  $\mathbf{A}$ , as shown in (4), naturally 232 become structurally sparse matrices. This sparsity reduces computational and memory overhead 233 during training, enabling faster gradient computation and parameter updates, while alleviating 234 communication overhead across distributed clients by transmitting only non-zero elements.

235 **Remark 3.3** (Sparsity Level Control). A key advantage of our formulation is its flexible control 236 over the sparsity level of local gradients, achieved by configuring the parameter  $k_i$  of the sketching 237 matrix set  $\mathcal{S}_i = \mathcal{S}(r, k_i)$ . This mechanism allows each client to tailor its local updates according to its 238 communication and computation resource constraints, ensuring efficient and scalable fine-tuning in 239 heterogeneous federated systems. Lowering  $k_i$  helps resource-constrained clients reduce computation 240 and communication overhead, while more capable clients can increase  $k_i$  to conduct more informative 241 local updates. Additionally, the distinction in sparsity level control between the proposed FSLoRA 242 and the FedBCGD algorithm (Liu et al., 2024) is elaborated in Appendix B.

243 **Remark 3.4** (Justification for the Choice of Random- $k$  Sketching). We adopt Random- $k$  sketching 244 due to its unbiasedness and the structured sparsity it induces. A detailed discussion and empirical 245 comparison with alternative sketching strategies are provided in Appendix C.

246 3.3 FSLoRA ALGORITHM  
247

248 Based on the formulation in (2), we propose a resource-adaptive algorithm termed FSLoRA for 249 collaborative LLM fine-tuning. FSLoRA allows each client to update submatrices of the original 250 modules  $\mathbf{B}$  and  $\mathbf{A}$  in each round. The server maintains a pair of global LoRA modules  $\mathbf{B}$  and  $\mathbf{A}$  251 and periodically updates them by aggregating sparse local updates received from distributed clients. 252 Specifically, the procedure of FSLoRA at each round is detailed below.

- 253 The server begins by sampling sketching matrices  $\{\mathbf{S}_i^t \sim \mathcal{S}_i\}_{i=1}^N$  for all clients, where  $\mathcal{S}_i$  represents 254 the set of possible sketching matrices for client  $i$ . These sketches are then sent to the corresponding 255 clients. Additionally, the server broadcasts the current global LoRA modules  $[\mathbf{B}^t; \mathbf{A}^t]$  to all clients. 256 Note that the communication load introduced by transmitting the sketching matrix is negligible 257 compared to global LoRA modules, as it involves only *binary sketching indices* (i.e., the diagonal 258 elements of the sketching matrix); see Appendix A for details.
- 259 Clients perform local fine-tuning using sketch  $\mathbf{S}_i^t$ . Specifically, guided by sketching matrix  $\mathbf{S}_i^t$ , the 260 update at client  $i$  during the  $h$ -th iteration of the  $t$ -th round is given by:

$$[\mathbf{B}_i^{t,h+1}; \mathbf{A}_i^{t,h+1}] = [\mathbf{B}_i^{t,h}; \mathbf{A}_i^{t,h}] - \gamma [\Delta \mathbf{B}_i^{t,h} (\mathbf{S}_i^t)^\top; (\mathbf{S}_i^t)^\top \Delta \mathbf{A}_i^{t,h}], \quad (5)$$

261 where  $\gamma$  denotes the learning rate and  $[\Delta \mathbf{B}_i^{t,h}; \Delta \mathbf{A}_i^{t,h}]$  is a shorthand representation for:

$$[\Delta \mathbf{B}_i^{t,h}; \Delta \mathbf{A}_i^{t,h}] = [\nabla \ell(\mathbf{W}_0 + \mathbf{B}_i^{t,h} \mathbf{S}_i^t \mathbf{A}_i^{t,h}, \xi_i^{t,h}) (\mathbf{A}_i^{t,h})^\top; (\mathbf{B}_i^{t,h})^\top \nabla \ell(\mathbf{W}_0 + \mathbf{B}_i^{t,h} \mathbf{S}_i^t \mathbf{A}_i^{t,h}, \xi_i^{t,h})].$$

266 The update direction in (5) corresponds to the negative stochastic gradient of  $\ell(\mathbf{W}_0 + \mathbf{BSA}, \xi)$  267 with respect to  $[\mathbf{B}; \mathbf{A}]$  for a given sketch  $\mathbf{S}_i^t$ , as established in Lemma 3.2. The total update for 268 client  $i$  during one round of training, consisting of  $H$  local steps, can be expressed as follows:

$$[\mathbf{B}_i^{t,H} - \mathbf{B}_i^{t,0}; \mathbf{A}_i^{t,H} - \mathbf{A}_i^{t,0}] = \left[ \gamma \left( \sum_{h=0}^{H-1} \Delta \mathbf{B}_i^{t,h} \right) (\mathbf{S}_i^t)^\top; \gamma (\mathbf{S}_i^t)^\top \left( \sum_{h=0}^{H-1} \Delta \mathbf{A}_i^{t,h} \right) \right]. \quad (6)$$

270 **Algorithm 1** Federated Sketching LoRA (FSLoRA)

---

271 **Require:** Base model  $\mathbf{W}_0$ , LoRA modules  $\mathbf{B}_0$  and  $\mathbf{A}_0$ , learning rate  $\gamma$ , and sketching set  $\{\mathcal{S}_i\}_{i=1}^N$

272 1: **for**  $t = 0, 1, \dots, T - 1$  **do**

273 2: Server samples sketching matrices  $\{\mathbf{S}_i^t \sim \mathcal{S}_i\}_{i=1}^N$  and sends them back to the clients

274 3: Server broadcasts the current global LoRA modules to the clients

275 4: **for**  $h = 0, 1, \dots, H - 1$  **do**

276 5: Clients update the local LoRA modules via (5)

277 6: **end for**

278 7: Clients upload the non-zero columns of  $(\mathbf{B}_i^{t,H} - \mathbf{B}_i^{t,0})$  and the non-zero rows of  $(\mathbf{A}_i^{t,H} - \mathbf{A}_i^{t,0})$

279 8: Server updates the global LoRA modules via (7)

280 9: **end for**

---

281  
282 From the above equation, we see that only the columns of  $\mathbf{B}$  and the rows of  $\mathbf{A}$  corresponding to  
283 the nonzero entries of  $\mathbf{S}_i^t$  are updated during the  $t$ -th round at client  $i$ . In essence,  $\mathbf{S}_i^t$  selectively  
284 activates specific columns of  $\mathbf{B}$  and rows of  $\mathbf{A}$  for each round. Afterward, clients transmit these  
285 nonzero columns and rows of the sparse model updates to the server.

286 • Using the sketch information, the server reconstructs the corresponding sparse matrices from the  
287 received updates and aggregates them to update the global model:

288

$$[\mathbf{B}^{t+1}; \mathbf{A}^{t+1}] = [\mathbf{B}^t; \mathbf{A}^t] + \frac{1}{N} \sum_{i=1}^N [\mathbf{B}_i^{t,H} - \mathbf{B}_i^{t,0}; \mathbf{A}_i^{t,H} - \mathbf{A}_i^{t,0}]. \quad (7)$$

289

290 Over training, random- $k$  sketching provides all columns and rows of the LoRA modules with uniform  
291 update frequency in expectation. The overall procedure of FSLoRA is summarized in Algorithm 1.

292 **Remark 3.5** (Aggregation). Existing works on federated LoRA primarily adopt two aggregation  
293 strategies: (1) aggregating the LoRA modules as  $[\mathbf{B}; \mathbf{A}]$  (e.g., vanilla Federated LoRA Zhang et al.  
294 (2024)), and (2) aggregating the product  $\mathbf{B}\mathbf{A}$  (e.g., FlexLoRA Bai et al. (2024)). Both methods have  
295 demonstrated effectiveness, as evidenced by their promising performance in prior studies. In this  
296 work, we adopt the former, as it introduces minimal overhead and retains the simplicity of LoRA.  
297 Additionally, we establish the convergence of FSLoRA under this aggregation choice in Section 4.  
298 We also demonstrate that FSLoRA is compatible with secure aggregation in Appendix D.

299 **Remark 3.6** (Computation, memory, and communication). The proposed FSLoRA introduces no  
300 additional operations compared to the vanilla Federated LoRA (Zhang et al., 2024), resulting in  
301 minimal overhead for both the server and the clients relative to other heterogeneous LoRA baselines  
302 (Bai et al., 2024; Wang et al., 2024). A more detailed comparison is provided in Appendix A.

## 303 3.4 COMPARISON WITH COMMUNICATION COMPRESSION

304 Although both the sketching approach in FSLoRA and communication compression (Kuo et al.,  
305 2024) reduce communication overhead, the sketching approach fundamentally differs from traditional  
306 compression techniques. Compression methods focus solely on reducing the transmission load,  
307 leaving the gradient computation and model updates unchanged from the vanilla Federated LoRA.  
308 FSLoRA goes beyond communication savings by also reducing gradient computation and model  
309 update overhead through sparse training. Notably, these two methods are orthogonal and can  
310 be combined to achieve greater efficiency. Specifically, the compression can be applied to the  
311 transmission of non-zero columns of  $\mathbf{B}$  and the non-zero rows of  $\mathbf{A}$  in FSLoRA to further enhance  
312 communication efficiency. We demonstrate the effectiveness of this combination in Appendix H.4.

## 313 4 ANALYSIS

314 In this section, we analyze the convergence of the proposed FSLoRA algorithm. We show that the  
315 iterate sequence generated by the FSLoRA algorithm converges to a stationary point of the function  
316 (2). Our analysis relies on the following notations.

317 **Notations:** We define  $\tilde{\ell}(\mathbf{B}, \mathbf{A}, \xi; \mathbf{S}) = \ell(\mathbf{W}_0 + \mathbf{B}\mathbf{S}\mathbf{A}, \xi)$  and  $\tilde{f}_i(\mathbf{B}, \mathbf{A}; \mathbf{S}) =$   
318  $\mathbb{E}_{\xi \sim \mathcal{D}_i} [\ell(\mathbf{W}_0 + \mathbf{B}\mathbf{S}\mathbf{A}, \xi)]$  for a given  $\mathbf{S}$  and  $f_i^S(\mathbf{B}, \mathbf{A}) = \mathbb{E}_{\mathbf{S} \sim \mathcal{S}_i} [\tilde{f}_i(\mathbf{B}, \mathbf{A}; \mathbf{S})]$ . For simplic-

324 ity, we denote  $\mathbf{X} = [\mathbf{B}; \mathbf{A}]$  and rewrite  $f(\mathbf{B}, \mathbf{A})$ ,  $f_i(\mathbf{B}, \mathbf{A})$ ,  $f^S(\mathbf{B}, \mathbf{A})$ ,  $f_i^S(\mathbf{B}, \mathbf{A})$ ,  $\tilde{f}_i(\mathbf{B}, \mathbf{A}; \mathbf{S})$ , and  
 325  $\tilde{\ell}(\mathbf{B}, \mathbf{A}, \xi; \mathbf{S})$  as  $f(\mathbf{X})$ ,  $f_i(\mathbf{X})$ ,  $f^S(\mathbf{X})$ ,  $f_i^S(\mathbf{X})$ ,  $\tilde{f}_i(\mathbf{X}; \mathbf{S})$ , and  $\tilde{\ell}(\mathbf{X}, \xi; \mathbf{S})$  respectively. In addition,  
 326 we use  $\|\cdot\|$  to denote the Frobenius norm.  
 327

328 We conduct analysis based on the following assumptions.

329 **Assumption 4.1.**  $f_i(\mathbf{X})$  is differentiable and  $L$ -smooth, i.e., there exists a positive constant  $L$  such  
 330 that  $\forall \mathbf{X}, \mathbf{Y}$ ,

$$331 \quad \|\nabla f_i(\mathbf{X}) - \nabla f_i(\mathbf{Y})\| \leq L\|\mathbf{X} - \mathbf{Y}\|, \forall i. \quad (8)$$

332 **Assumption 4.2.**  $\nabla_{\mathbf{X}} \tilde{\ell}(\mathbf{X}, \xi; \mathbf{S})$  is an unbiased estimate of  $\nabla_{\mathbf{X}} f_i^S(\mathbf{X})$  and its variance is bounded as  
 333

$$334 \quad \mathbb{E}\|\nabla_{\mathbf{X}} \tilde{\ell}(\mathbf{X}, \xi; \mathbf{S}) - \nabla_{\mathbf{X}} f_i^S(\mathbf{X})\|^2 \leq \rho\|\nabla_{\mathbf{X}} f_i^S(\mathbf{X})\|^2 + \sigma^2, \forall i, \quad (9)$$

335 where the expectation is computed over  $\xi \sim \mathcal{D}_i$  and  $\mathbf{S} \sim \mathcal{S}_i$ .

336 **Assumption 4.3.** The gradient dissimilarity between the global loss  $f^S(\mathbf{X})$  and each local loss  
 337  $f_i^S(\mathbf{X})$  satisfies

$$338 \quad \|\nabla_{\mathbf{X}} f_i^S(\mathbf{X}) - \nabla_{\mathbf{X}} f^S(\mathbf{X})\|^2 \leq c_h \|\nabla_{\mathbf{X}} f^S(\mathbf{X})\|^2 + \delta_h^2, \forall i, \quad (10)$$

340 where  $c_h \geq 0$  and  $f^S(\mathbf{X}) = \frac{1}{N} \sum_{i=1}^N f_i^S(\mathbf{X})$ .

342 Assumption 4.1 is standard in optimization literature (Bottou et al., 2018; Fang et al., 2024; Bubeck  
 343 et al., 2015). Assumptions 4.2 and 4.3 are commonly adopted in federated learning to bound sampling  
 344 randomness and data heterogeneity (Fang et al., 2022; Yi et al., 2022). We further provide an  
 345 empirical validation in Appendix E, showing that Assumptions 4.2 and 4.3 are reasonable within the  
 346 LLM fine-tuning scenario. Building on these assumptions, we analyze the convergence behavior of  
 347 FSLoRA. Our main results are summarized in the following theorem.

348 **Theorem 4.4.** Suppose that Assumptions 4.1-4.3 hold, then there exists a learning rate  $\gamma \leq$   
 349  $\min\{\frac{N}{24\rho(c_h+1)H\bar{L}}, \frac{1}{8\sqrt{\bar{L}L(\rho+1)(c_h+1)H}}, \frac{1}{H}\}$  such that the iterates  $\{\mathbf{X}^t\}$  generated by FSLoRA satisfy

$$351 \quad \frac{1}{T} \sum_{t=0}^{T-1} \mathbb{E} \|\nabla_{\mathbf{X}} f^S(\mathbf{X}^t)\|^2 \leq 8 \frac{\sqrt{\bar{L}\mathcal{F}_0\sigma_\rho^2}}{\sqrt{NTH}} + 10(\tilde{L}L)^{\frac{1}{3}} \left( \frac{\mathcal{F}_0\sigma_\rho}{T} \right)^{\frac{2}{3}} + \frac{4\mathcal{F}_0}{T}, \quad (11)$$

354 where  $\sigma_\rho^2 = \sigma^2 + 3(\rho+1)\sigma_h^2$ ,  $\bar{L} = \left(\frac{1}{N} \sum_{i=1}^N \frac{r}{k_i}\right) L$ ,  $\tilde{L} = \left(\frac{1}{N} \sum_{i=1}^N \frac{r^2}{k_i^2}\right) L$  and  $\mathcal{F}_0 = f^S(\mathbf{X}^0) - f^*$   
 355 with  $f^*$  denoting the lower bound of  $f^S(\mathbf{X})$ .

357 **Technical highlights of Theorem 4.4:** A key step in the proof of Theorem 4.4 is characterizing  
 358 the impact of the sketching mechanism on the optimization landscape. Our analysis reveals how  
 359 the sketching operation modifies the smoothness properties of the objective, introducing scaled  
 360 smoothness constants,  $\frac{r}{k_i}L$  and  $\frac{r^2}{k_i^2}L$ , which directly influence the convergence behavior. Further  
 361 details are presented in Appendix J.3.

363 **Discussion:** Theorem 4.4 establishes an upper bound on the convergence of the proposed FSLoRA  
 364 algorithm. The parameters  $\bar{L}$  and  $\tilde{L}$  provide insight into how the sketching operation influences the  
 365 convergence rate. Increasing  $k_i$  would lead to a faster convergence for FSLoRA. However, this comes  
 366 at the cost of increased communication and computational overhead for client  $i$ , indicating a trade-off  
 367 in the selection of the sketching ratios. Additionally, the upper bound vanishes as  $T \rightarrow \infty$ . Moreover,  
 368 the rate at which the bound diminishes is dominated by the first term, which recovers the convergence  
 369 behavior of FedAvg (Yu et al., 2019; Khaled et al., 2020; Karimireddy et al., 2020) as the sketching  
 370 ratio  $k_i/r \rightarrow 1$  (i.e.,  $\bar{L} = L$ ). This highlights the tightness of our analysis and shows that FSLoRA  
 371 retains the convergence guarantees of vanilla Federated LoRA in the limit.

## 373 5 EXPERIMENTS

375 Our experiments focus on RoBERTa (125M) (Liu, 2019) and LLaMA-3.2-3B (Dubey et al., 2024),  
 376 which represent typical model sizes suitable for client-side deployment, as well as the LLaMA-7B  
 377 model to reflect large-scale scenarios. For RoBERTa and LLaMA-3.2-3B models, we fine-tune  
 and evaluate them on the GLUE (Wang, 2018) and commonsense reasoning benchmark (Hu et al.,

378 Table 5.1: Testing accuracy over 3 independent runs on GLUE and commonsense reasoning benchmarks.  
 379 FSLoRA achieves a notable improvement in average performance compared to the baselines.  
 380

GLUE benchmark (RoBERTa model)										
Method	GPU hours	QNLI	MRPC	CoLA	MNLI	RTE	SST-2	QQP	Avg.	
HeteroLoRA	10.7h	87.5 $\pm$ 0.5	84.4 $\pm$ 0.9	75.3 $\pm$ 1.2	66.3 $\pm$ 0.8	69.0 $\pm$ 1.7	89.5 $\pm$ 0.0	85.3 $\pm$ 0.1	79.6	
FlexLoRA	12.6h	88.5 $\pm$ 0.2	81.2 $\pm$ 0.4	77.5 $\pm$ 1.2	63.0 $\pm$ 0.5	62.2 $\pm$ 1.9	92.8 $\pm$ 0.4	87.4 $\pm$ 0.1	78.9	
FLoRA	12.3h	87.2 $\pm$ 0.3	78.1 $\pm$ 0.7	77.4 $\pm$ 1.7	74.6 $\pm$ 0.5	54.4 $\pm$ 2.1	93.4 $\pm$ 0.1	87.1 $\pm$ 0.3	78.9	
FSLoRA	10.9h	88.0 $\pm$ 0.3	87.3 $\pm$ 0.2	82.2 $\pm$ 0.5	76.4 $\pm$ 0.2	69.8 $\pm$ 1.2	93.5 $\pm$ 0.1	85.8 $\pm$ 0.1	83.3	

Commonsense reasoning benchmark (LLaMA-3.2-3B model)										
Method	GPU hours	ARC-c	ARC-e	BoolQ	HellaSwag	OBQA	PIQA	SIQA	WinoGrande	Avg.
HeteroLoRA	43.7h	73.4 $\pm$ 0.3	86.6 $\pm$ 0.2	65.8 $\pm$ 0.5	73.0 $\pm$ 0.5	71.4 $\pm$ 0.3	80.9 $\pm$ 0.7	73.8 $\pm$ 0.3	72.0 $\pm$ 0.3	74.6
FlexLoRA	68.3h	74.2 $\pm$ 0.3	86.7 $\pm$ 0.6	68.6 $\pm$ 0.8	79.4 $\pm$ 0.7	75.8 $\pm$ 0.4	81.0 $\pm$ 0.3	75.9 $\pm$ 0.4	77.9 $\pm$ 0.3	77.4
FLoRA	49.8h	68.3 $\pm$ 0.6	83.1 $\pm$ 0.5	65.8 $\pm$ 0.9	77.2 $\pm$ 0.5	74.2 $\pm$ 0.3	80.5 $\pm$ 0.6	76.1 $\pm$ 0.5	71.5 $\pm$ 0.5	74.6
FSLoRA	44.3h	76.1 $\pm$ 0.4	87.2 $\pm$ 0.5	69.3 $\pm$ 0.7	82.2 $\pm$ 1.1	80.7 $\pm$ 0.6	84.0 $\pm$ 0.2	76.8 $\pm$ 0.0	79.1 $\pm$ 0.2	79.4

392 2023), respectively. For the LLaMA-7B model, we utilize Wizard, Dolly-15k, and Alpaca datasets,  
 393 where the results are reported in Appendix G. Similar to (Zhang et al., 2024; Wang et al., 2024), we  
 394 adopt Dirichlet-based partitioning for dataset splits. All the experiments are conducted on a cluster  
 395 equipped with 4 NVIDIA A100 GPUs, each with 40 GB of memory. The number of clients is set  
 396 to 20 in the main manuscript, and to 50 and 100 in Appendix F. Further details are provided in the  
 397 Appendix I. The implementation code for this project is included in the supplementary material.

## 398 5.1 MAIN RESULTS UNDER HETEROGENEOUS LoRA SETUP

400 **Performance comparison with baselines:** We consider three state-of-the-art baselines listed in  
 401 Section 2.2. For FSLoRA, the rank of the global LoRA modules is fixed as  $r = 64$ , while the sketching  
 402 ratio for client  $i$  is sampled from the set  $\{0.125, 0.25, 0.5, 0.75\}$ . For a fair comparison, we apply  
 403 the same rank configuration to all baseline methods. Table 5.1 presents the performance of FSLoRA  
 404 and baseline methods. Across both settings, FSLoRA consistently achieves superior accuracy while  
 405 maintaining low GPU hours. In the GLUE & RoBERTa task, FSLoRA outperforms all baselines  
 406 on average, with significant gains in MRPC, CoLA, and MNLI. In the commonsense reasoning &  
 407 LLaMA task, which introduces higher model complexity, FSLoRA also delivers the best overall  
 408 performance. Notably, FSLoRA achieves this while preserving computational efficiency comparable  
 409 to HeteroLoRA as reflected in GPU hours. These results highlight FSLoRA’s effectiveness and  
 410 scalability in heterogeneous LoRA fine-tuning scenarios.

411 **Evaluation under broader heterogeneity, increased number of clients, and larger model:** In  
 412 Appendix F, we extend our evaluation to 50 and 100 clients, incorporating greater diversity in clients’  
 413 communication and computation capabilities, as well as varying levels of data heterogeneity. In  
 414 Appendix G, we further assess the effectiveness of our method on the LLaMA-7B model.

## 415 5.2 ABLATION STUDY

416 **Impact of sketching:** In Figures 2 and 3(a), we compare the performance of FSLoRA with and  
 417 without sketching on fine-tuning the RoBERTa model and the LLaMA-3.2-3B model, respectively.  
 418 Notably, FSLoRA without sketching is equivalent to the vanilla Federated LoRA. For FSLoRA with  
 419 sketching, we apply a uniform sketching ratio of  $k_i/r = 0.5$  across all distributed clients. The upload  
 420 budget for each client is set to 100 and 80 times the size of the full global LoRA modules at the  
 421 corresponding rank for the RoBERTa and the LLaMA-3.2-3B models, respectively. As shown in  
 422 Figures 2 and 3(a), both FSLoRA with and without sketching achieve higher accuracy when the rank  
 423  $r$  increases due to the availability of more tunable parameters. In addition, FSLoRA consistently  
 424 outperforms its non-sketched counterpart across all the ranks and datasets. The use of sketching  
 425 increases the communication frequency for clients under the same communication budget, thereby  
 426 facilitating the optimization process and enhancing fine-tuning efficiency.

427 **Impact of the global rank:** In Figure 3(b), we investigate the impact of the rank of the global LoRA  
 428 modules on FSLoRA’s performance. We vary the rank of the global LoRA modules while keeping  
 429 the rank of submatrices updated by the clients to be consistent (i.e.,  $k_i = 8$ ). This ensures that the  
 430 communication and computational resources on the client side remain unchanged. As illustrated in  
 431 Figure 3(b), FSLoRA maintains stable convergence across all the configurations. Moreover, FSLoRA

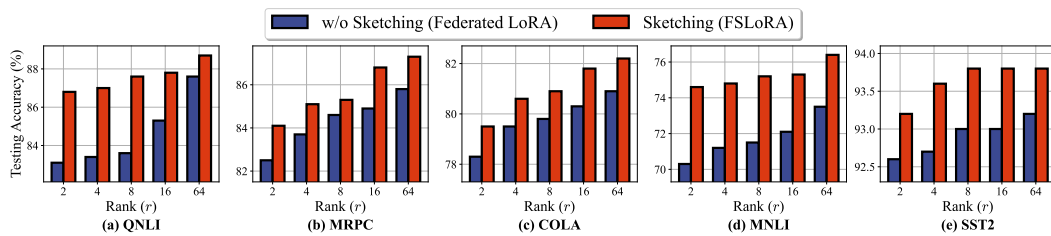
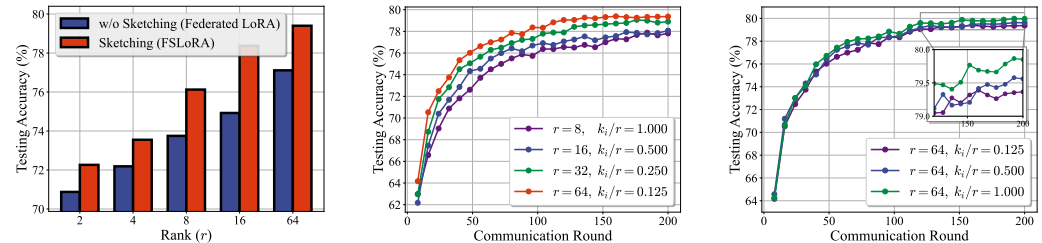


Figure 2: Comparison between FSLoRA with and without sketching (the latter equivalent to Federated LoRA) where the upload budget for clients is set to  $100 \times$  the size of the global LoRA modules at each rank. FSLoRA obtains a better performance, validating its communication efficiency.



(a) Comparison of FSLoRA with and without sketching, with an upload budget  $80 \times$  the size of the global LoRA modules at each rank. (b) Impact of the rank of global LoRA modules on FSLoRA, given a fixed rank  $k_i$  for the updated sub-global LoRA modules at the clients. (c) Impact of the sketching ratio on FSLoRA's performance under a fixed rank  $r = 64$  for the global LoRA modules.

Figure 3: Fine-tuning the LLaMA-3.2-3B model on the commonsense reasoning benchmark. The results are averaged over eight tasks, illustrating FSLoRA's ability to maintain strong performance while adapting to different rank and sketching configurations.

demonstrates improved performance as the global rank increases. This observation confirms that the proposed sketching mechanism enables resource-constrained systems to reap the benefits of a higher global rank, striking an effective balance between efficiency and performance.

**Impact of sketching ratio:** Finally, we investigate the impact of the sketching ratio on FSLoRA's performance by maintaining a constant global LoRA rank  $r = 64$  while varying the sketching ratio  $k_i/r$  in the range  $\{0.125, 0.5, 1\}$ . As shown in Figure 3(c), there is a slight performance degradation as the sketching ratio decreases, which is consistent with our theoretical analysis. This reflects an inherent tradeoff: while a larger sketching ratio improves convergence and accuracy, a smaller ratio reduces both computational and communication overhead. Notably, the observed degradation remains minor, highlighting FSLoRA's ability to maintain strong performance even under constrained resources. This demonstrates its effectiveness in balancing efficiency and accuracy, making it well-suited for resource-limited scenarios.

**Further experiments:** Results with more clients under broader heterogeneity, as well as with a larger model, are reported in Appendix F and Appendix G, respectively. Appendix H.1 provides detailed per-task comparisons on the commonsense reasoning benchmark corresponding to Figures 3(a) and 3(b). The impact of varying the number of local updates  $H$  is studied in Appendix H.2, while the extension to dynamic sketching ratios is presented in Appendix H.3. Finally, Appendix H.4 demonstrates the synergistic effect of integrating compression with sketching.

## 6 CONCLUSION

We have proposed FSLoRA, a novel collaborative LLM fine-tuning framework that introduces a sketching mechanism to enhance both performance and efficiency in resource-constrained systems. By maintaining large-rank LoRA modules on the server and allowing clients to selectively update submatrices based on the sketching ratios, FSLoRA effectively adapts to heterogeneous communication and computational constraints. We provide a rigorous convergence analysis of FSLoRA that characterizes how the sketching ratios affect the convergence rate. Finally, we confirmed the effectiveness of FSLoRA through extensive experiments across multiple datasets and models.

486  
487  
**LIMITATION**488  
489  
490  
491  
A potential limitation is that our paper is primarily theoretical. Extending the proposed techniques to  
practical network environments and evaluating their behavior under unstable connections, delayed  
clients, and latency fluctuations remains an important direction for future work.492  
493  
**REPRODUCIBILITY STATEMENT**494  
495  
496  
497  
498  
This paper provides all the necessary information to reproduce the main experimental results. The  
datasets used are publicly available, while the model architectures, hyperparameters, and training  
details are documented in Section 5. The full implementation code is included in the supplementary  
material of our submission.499  
500  
**LLM USAGE**501  
502  
503  
504  
505  
506  
We used ChatGPT (GPT-5), as an assistive tool only for improving the clarity and readability of the  
manuscript. The LLM was employed to polish grammar and rephrase sentences for conciseness. It  
was not used for research ideation, methodological design, and experimental implementation. All  
scientific content, including problem formulation, algorithm development, analysis, and experiments,  
was entirely conceived and executed by the authors.507  
508  
**REFERENCES**509  
510  
J. Bai, D. Chen, B. Qian, L. Yao, and Y. Li. Federated fine-tuning of large language models under  
heterogeneous tasks and client resources. *arXiv preprint arXiv:2402.11505*, 2024.  
511  
512  
Y. Bisk, R. Zellers, J. Gao, Y. Choi, et al. Piqa: Reasoning about physical commonsense in natural  
language. In *Proceedings of the AAAI conference on artificial intelligence*, volume 34, pages  
7432–7439, 2020.  
513  
514  
515  
L. Bottou, F. E. Curtis, and J. Nocedal. Optimization methods for large-scale machine learning. *SIAM*  
*review*, 60(2):223–311, 2018.  
516  
517  
518  
S. Bubeck et al. Convex optimization: Algorithms and complexity. *Foundations and Trends® in*  
*Machine Learning*, 8(3-4):231–357, 2015.  
519  
520  
521  
Y. Byun and J. Lee. Towards federated low-rank adaptation of language models with rank hetero-  
geneity. *arXiv preprint arXiv:2406.17477*, 2024.  
522  
523  
524  
N. Charalambides and A. Mazumdar. Distributed hybrid sketching for l2-embeddings. *arXiv preprint*  
*arXiv:2412.20301*, 2024.  
525  
526  
C. Chen, X. Feng, J. Zhou, J. Yin, and X. Zheng. Federated large language model: A position paper.  
*arXiv preprint arXiv:2307.08925*, 2023.  
527  
528  
Y. J. Cho, L. Liu, Z. Xu, A. Fahrezi, and G. Joshi. Heterogeneous LoRA for federated fine-tuning of  
on-device foundation models. *arXiv preprint arXiv:2401.06432*, 2024.  
529  
530  
531  
C. Clark, K. Lee, M.-W. Chang, T. Kwiatkowski, M. Collins, and K. Toutanova. Boolq: Exploring  
the surprising difficulty of natural yes/no questions. *arXiv preprint arXiv:1905.10044*, 2019.  
532  
533  
534  
P. Clark, I. Cowhey, O. Etzioni, T. Khot, A. Sabharwal, C. Schoenick, and O. Tafjord. Think you have  
solved question answering? try arc, the ai2 reasoning challenge. *arXiv preprint arXiv:1803.05457*,  
2018.  
535  
536  
537  
Y. Demidovich, G. Malinovsky, E. Shulgin, and P. Richtárik. Mast: Model-agnostic sparsified  
training. *arXiv preprint arXiv:2311.16086*, 2023.  
538  
539  
A. Dubey, A. Jauhri, A. Pandey, A. Kadian, A. Al-Dahle, A. Letman, A. Mathur, A. Schelten, A. Yang,  
A. Fan, et al. The llama 3 herd of models. *arXiv preprint arXiv:2407.21783*, 2024.

540 D. Fan, B. Messmer, and M. Jaggi. On-device collaborative language modeling via a mixture of  
 541 generalists and specialists. *arXiv preprint arXiv:2409.13931*, 2024.

542

543 W. Fang, Z. Yu, Y. Jiang, Y. Shi, C. N. Jones, and Y. Zhou. Communication-efficient stochastic  
 544 zeroth-order optimization for federated learning. *IEEE Transactions on Signal Processing*, 70:  
 545 5058–5073, 2022.

546 W. Fang, D.-J. Han, E. Chen, S. Wang, and C. G. Brinton. Hierarchical federated learning with  
 547 multi-timescale gradient correction. *arXiv preprint arXiv:2409.18448*, 2024.

548

549 R. M. Gower and P. Richtárik. Randomized iterative methods for linear systems. *SIAM Journal on  
 550 Matrix Analysis and Applications*, 36(4):1660–1690, 2015.

551 P. Guo, S. Zeng, Y. Wang, H. Fan, F. Wang, and L. Qu. Selective aggregation for low-rank adaptation  
 552 in federated learning. *arXiv preprint arXiv:2410.01463*, 2025.

553

554 E. J. Hu, Y. Shen, P. Wallis, Z. Allen-Zhu, Y. Li, S. Wang, L. Wang, and W. Chen. LoRA: Low-rank  
 555 adaptation of large language models. *arXiv preprint arXiv:2106.09685*, 2021.

556

557 Z. Hu, L. Wang, Y. Lan, W. Xu, E.-P. Lim, L. Bing, X. Xu, S. Poria, and R. K.-W. Lee. LLM-adapters:  
 558 An adapter family for parameter-efficient fine-tuning of large language models. *arXiv preprint  
 559 arXiv:2304.01933*, 2023.

560 D. Kalajdzievski. A rank stabilization scaling factor for fine-tuning with LoRA. *arXiv preprint  
 561 arXiv:2312.03732*, 2023.

562

563 S. P. Karimireddy, S. Kale, M. Mohri, S. Reddi, S. Stich, and A. T. Suresh. Scaffold: Stochastic  
 564 controlled averaging for federated learning. In *International conference on machine learning*,  
 565 pages 5132–5143. PMLR, 2020.

566

567 A. Khaled, K. Mishchenko, and P. Richtárik. Tighter theory for local sgd on identical and heteroge-  
 568 neous data. In *International Conference on Artificial Intelligence and Statistics*, pages 4519–4529.  
 569 PMLR, 2020.

570

571 A. Koloskova, N. Loizou, S. Boreiri, M. Jaggi, and S. Stich. A unified theory of decentralized sgd  
 572 with changing topology and local updates. In *International conference on machine learning*, pages  
 573 5381–5393. PMLR, 2020.

574

575 J. Koo, M. Jang, and J. Ok. Towards robust and efficient federated low-rank adaptation with  
 576 heterogeneous clients. *arXiv preprint arXiv:2410.22815*, 2024.

577

578 K. Kuo, A. Raje, K. Rajesh, and V. Smith. Federated LoRA with sparse communication. *arXiv  
 579 preprint arXiv:2406.05233*, 2024.

580

581 B. Lester, R. Al-Rfou, and N. Constant. The power of scale for parameter-efficient prompt tuning.  
 582 *arXiv preprint arXiv:2104.08691*, 2021.

583

584 X. L. Li and P. Liang. Prefix-tuning: Optimizing continuous prompts for generation. *arXiv preprint  
 585 arXiv:2101.00190*, 2021.

586

587 J. Liu, F. Shang, Y. Liu, H. Liu, Y. Li, and Y. Gong. FedBCGD: Communication-efficient accelerated  
 588 block coordinate gradient descent for federated learning. In *Proceedings of the 32nd ACM  
 589 International Conference on Multimedia*, pages 2955–2963, 2024.

590

591 Y. Liu. Roberta: A robustly optimized bert pretraining approach. *arXiv preprint arXiv:1907.11692*,  
 592 364, 2019.

593

594 B. McMahan, E. Moore, D. Ramage, S. Hampson, and B. A. y Arcas. Communication-efficient  
 595 learning of deep networks from decentralized data. In *Artificial intelligence and statistics*, pages  
 596 1273–1282. PMLR, 2017.

597

598 T. Mihaylov, P. Clark, T. Khot, and A. Sabharwal. Can a suit of armor conduct electricity? a new  
 599 dataset for open book question answering. *arXiv preprint arXiv:1809.02789*, 2018.

594 J. Nicolas, M. Maouche, S. B. Mokhtar, and M. Coates. Communication efficient, differentially private  
 595 distributed optimization using correlation-aware sketching. *arXiv preprint arXiv:2507.03545*, 2025.  
 596

597 K. Sakaguchi, R. L. Bras, C. Bhagavatula, and Y. Choi. Winogrande: An adversarial winograd  
 598 schema challenge at scale. *Communications of the ACM*, 64(9):99–106, 2021.

599 M. Sap, H. Rashkin, D. Chen, R. LeBras, and Y. Choi. Socialiqa: Commonsense reasoning about  
 600 social interactions. *arXiv preprint arXiv:1904.09728*, 2019.  
 601

602 T. Sarlos. Improved approximation algorithms for large matrices via random projections. In *2006*  
 603 *47th annual IEEE symposium on foundations of computer science (FOCS'06)*, pages 143–152.  
 604 IEEE, 2006.

605 M. Shrivastava, B. Isik, Q. Li, S. Koyejo, and A. Banerjee. Sketching for distributed deep learning: A  
 606 sharper analysis. *Advances in Neural Information Processing Systems*, 37:6417–6447, 2024.  
 607

608 R. Shuttleworth, J. Andreas, A. Torralba, and P. Sharma. LoRA vs full fine-tuning: An illusion of  
 609 equivalence. *arXiv preprint arXiv:2410.21228*, 2024.

610 Y. Sun, Z. Li, Y. Li, and B. Ding. Improving LoRA in privacy-preserving federated learning. *arXiv*  
 611 *preprint arXiv:2403.12313*, 2024.  
 612

613 A. Wang. Glue: A multi-task benchmark and analysis platform for natural language understanding.  
 614 *arXiv preprint arXiv:1804.07461*, 2018.

615 J. Wang, Q. Liu, H. Liang, G. Joshi, and H. V. Poor. A novel framework for the analysis and design of  
 616 heterogeneous federated learning. *IEEE Transactions on Signal Processing*, 69:5234–5249, 2021.  
 617

618 R. Wang, Y. Ouyang, and W. Xu. Iterative double sketching for faster least-squares optimization. In  
 619 *International Conference on Machine Learning*, pages 22935–22963. PMLR, 2022.

620 Z. Wang, Z. Shen, Y. He, G. Sun, H. Wang, L. Lyu, and A. Li. FLoRA: Federated fine-tuning large  
 621 language models with heterogeneous low-rank adaptations. *arXiv preprint arXiv:2409.05976*,  
 622 2024.

623 R. Ye, W. Wang, J. Chai, D. Li, Z. Li, Y. Xu, Y. Du, Y. Wang, and S. Chen. Openfedllm: Training  
 624 large language models on decentralized private data via federated learning. In *Proceedings of the*  
 625 *30th ACM SIGKDD Conference on Knowledge Discovery and Data Mining*, pages 6137–6147,  
 626 2024.

627 X. Yi, S. Zhang, T. Yang, and K. H. Johansson. Zeroth-order algorithms for stochastic distributed  
 628 nonconvex optimization. *Automatica*, 142:110353, 2022.

629 H. Yu, S. Yang, and S. Zhu. Parallel restarted sgd with faster convergence and less communication:  
 630 Demystifying why model averaging works for deep learning. In *Proceedings of the AAAI conference*  
 631 *on artificial intelligence*, volume 33, pages 5693–5700, 2019.

632 R. Zellers, A. Holtzman, Y. Bisk, A. Farhadi, and Y. Choi. Hellaswag: Can a machine really finish  
 633 your sentence? *arXiv preprint arXiv:1905.07830*, 2019.

634 J. Zhang, S. Vahidian, M. Kuo, C. Li, R. Zhang, T. Yu, G. Wang, and Y. Chen. Towards building the  
 635 federatededgpt: Federated instruction tuning. In *ICASSP 2024-2024 IEEE International Conference*  
 636 *on Acoustics, Speech and Signal Processing (ICASSP)*, pages 6915–6919. IEEE, 2024.  
 637

638

639

640

641

642

643

644

645

646

647

# Appendix

648	<b>A Comparison of Computation, Memory, and Communication</b>	<b>14</b>
649		
650		
651	<b>B Difference between FSLoRA and FedBCGD</b>	<b>15</b>
652		
653		
654	<b>C Justification for Random-<math>k</math> Sketching</b>	<b>15</b>
655		
656		
657	<b>D Compatibility of FSLoRA with Secure Aggregation</b>	<b>16</b>
658		
659		
660	<b>E Empirical Validation of Assumptions</b>	<b>16</b>
661		
662	<b>F Evaluation under Broader Heterogeneity and Increased Number of Clients</b>	<b>17</b>
663		
664	F.1 Increasing Resource Heterogeneity and the Number of Clients . . . . .	17
665	F.2 Further Increasing the Number of Clients . . . . .	18
666	F.3 Varying the Level of Data Heterogeneity . . . . .	19
667		
668		
669	<b>G Experiments on Qwen2.5-1.5B-Instruct and LLaMA-7B</b>	<b>19</b>
670		
671	<b>H Further Experiments</b>	<b>20</b>
672	H.1 Further Details on the Ablation Study . . . . .	20
673	H.2 Impact of Local Updates . . . . .	20
674	H.3 Dynamic Sketching Ratios . . . . .	22
675	H.4 Integration of Sketching and Top- $k$ Compression . . . . .	22
676		
677		
678		
679	<b>I Implementation Details</b>	<b>23</b>
680	I.1 Details on Hyperparameters . . . . .	23
681	I.2 Details on Datasets . . . . .	23
682	I.2.1 GLUE Benchmark . . . . .	23
683	I.2.2 Commonsense Reasoning Benchmark . . . . .	24
684		
685		
686		
687	<b>J Proof of the Theoretical Results</b>	<b>26</b>
688	J.1 Preliminaries . . . . .	26
689	J.2 Proof of Lemma 3.2 . . . . .	27
690	J.3 Proof of Theorem 4.4 . . . . .	27
691	J.4 Proof of Proposition J.5 . . . . .	30
692		
693		
694		
695		
696		
697		
698		
699		
700		
701		

## 702 A COMPARISON OF COMPUTATION, MEMORY, AND COMMUNICATION

704 **Computation and memory:** Let  $P$  and  $q$  denote the memory cost of the full model and the global  
 705 LoRA module (rank  $r$ ), respectively. The computational cost is expressed with the big O notation.  
 706 Forward and backward computations, as well as activation memory, are omitted as they are identical  
 707 across all the considered methods. The results are summarized in Tables A.1 and A.2, where  $m$  and  $n$   
 708 denote the shape of the base model,  $k_i$  denotes the LoRA rank for client  $i$ ,  $H$  denotes the number of  
 709 iterations per round, and  $N$  is the number of clients. Additionally, the results for the vanilla Federated  
 710 LoRA, denoted as FedLoRA, are reported under the case of homogeneous LoRA ranks, i.e.,  $k_i = r$ .

711  
712 Table A.1: Client-side computation load and memory usage comparison.

714 Method	715 Memory	716 Computation (per round)
FedLoRA	$P + q$	$\mathcal{O}(Hr(m + n))$
HeteroLoRA	$P + \frac{k_i}{r}q$	$\mathcal{O}(Hk_i(m + n))$
FlexLoRA	$P + \frac{k_i}{r}q$	$\mathcal{O}(Hk_i(m + n))$
FLoRA	$P + \max \left\{ \sum_{i=1}^N \frac{k_i}{r}q, P \right\}$	$\mathcal{O} \left( Hk_i(m + n) \right) + \left( \sum_{i=1}^N k_i \right) mn + mn$
FSLoRA	$P + \frac{k_i}{r}q$	$\mathcal{O}(Hk_i(m + n))$

721  
722 Table A.2: Server-side computation load and memory usage comparison.

725 Method	726 Memory	727 Computation (per round)
FedLoRA	$Nq$	$\mathcal{O}(N(m + n)r)$
HeteroLoRA	$\sum_{i=1}^N \frac{k_i}{r}q$	$\mathcal{O}(N(m + n)r)$
FlexLoRA	$\max \left\{ \sum_{i=1}^N \frac{k_i}{r}q, 2P \right\}$	$\mathcal{O} \left( \left( \sum_{i=1}^N k_i \right) mn + Nmn + \min\{m, n\}mn \right)$
FLoRA	$\sum_{i=1}^N \frac{k_i}{r}q$	$\mathcal{O} \left( \left( \sum_{i=1}^N k_i \right) (m + n) \right)$
FSLoRA	$\sum_{i=1}^N \frac{k_i}{r}q$	$\mathcal{O}(N(m + n)r)$

733 As shown in Tables A.1 and A.2, FSLoRA matches HetLoRA in both computation and memory cost.  
 734 FLoRA introduces additional client-side overhead due to merging LoRA modules. FlexLoRA incurs  
 735 extra server-side costs from conducting SVD on the full model. In summary, FSLoRA guarantees  
 736 convergence with minimum overhead.

737 **Communication:** We detailed the communication load for baselines and our methods in Table A.3,  
 738 where  $q$  denotes the communication cost of a global LoRA module with rank  $r$ ,  $k_i$  denotes the local  
 739 LoRA rank for client  $i$ ,  $m$  and  $n$  denote the shape of the base model, and  $N$  denotes the number of  
 740 clients.

741  
742 Table A.3: Communication complexity, assuming float 32 parameters and binary sketching indices.

	FedLoRA	HeteroLoRA	FlexLoRA	FLoRA	FSLoRA
Uplink	$q$	$\frac{k_i}{r}q$	$\frac{k_i}{r}q$	$\frac{k_i}{r}q$	$\frac{k_i}{r}q$
Downlink	$q$	$q$	$q$	$\sum_{i=1}^N \frac{k_i}{r}q$	$q \left( 1 + \frac{Nr}{32mn} \right)$

748 For the uplink, all four heterogeneous LoRA algorithms incur the same communication overhead for  
 749 transmitting updated local LoRA modules, which is lower than that of FedLoRA. For the downlink,  
 750 FLoRA requires broadcasting the stacked LoRA modules, while HeteroLoRA and FlexLoRA broad-  
 751 cast the updated global LoRA modules. FSLoRA, on the other hand, broadcasts both the global LoRA  
 752 modules and additional sketching matrices. The extra communication introduced by the sketching  
 753 matrices is negligible compared to that of the global LoRA modules, as it consists only of *binary*  
 754 *sketching indices* (i.e., the diagonal elements of the sketching matrix). For instance, in the case of  
 755 the LLaMA-3.2-3B model under our experimental LoRA configuration, the global LoRA modules  
 contain 66,060,288 parameters, equivalent to approximately 252 MB when using float32. With a

756 global rank of  $r = 64$ , the sketching indices require only 64 bits per client, covering all LoRA layers.  
 757 Even with 100 clients, the total sketching overhead is merely 0.78 KB, which accounts for only  
 758 0.0003% of the global LoRA modules.  
 759

## 760 B DIFFERENCE BETWEEN FSLoRA AND FEDBCGD

762 Both FSLoRA and federated block coordinate gradient descent (FedBCGD) (Liu et al., 2024) are  
 763 motivated by client heterogeneity but are designed for fundamentally different deployment contexts.  
 764 FedBCGD partitions the full model  $\mathbf{x} = [\mathbf{x}_1, \dots, \mathbf{x}_N, \mathbf{x}_s]$ , assigning each block  $\mathbf{x}_j$  to a subset of  
 765 clients with similar resource constraints, while the shared block  $\mathbf{x}_s$  is optimized across all clients.  
 766 While this block-partitioning strategy is effective for smaller models, it relies on explicit and static  
 767 allocation, which can limit scalability and flexibility. As such, FedBCGD and similar block coordinate  
 768 methods based on the full model are less suitable for federated LLM fine-tuning.  
 769

770 FSLoRA, in contrast, builds on LoRA and introduces sparse diagonal sketching. Given a sketch  
 771 matrix  $\mathbf{S}$ , the gradients of the loss  $\ell(\mathbf{W}_0 + \mathbf{BSA}, \xi)$  with respect to the LoRA matrices  $\mathbf{B}$  and  $\mathbf{A}$   
 772 are sparse: only selected columns of  $\mathbf{B}$  and rows of  $\mathbf{A}$  are updated in each round. By configuring  
 773 the rank and sparsity of the sketch matrix  $\mathbf{S}$ , FSLoRA flexibly controls both the computational and  
 774 communication load per client, enabling adaptation to heterogeneous client capabilities.  
 775

776 The distinctions between FedBCGD and FSLoRA are summarized in Table B.1. To wrap up, these  
 777 two algorithms are tailored for distinct purposes and deployment contexts.  
 778

779 Table B.1: Conceptual distinctions between FSLoRA and FedBCGD.  
 780

781 Aspect	782 FedBCGD	783 FSLoRA
784 Partition Type	785 Explicit & static	786 Random & sketching-based
787 Model Scope	788 Full model	789 LoRA modules
790 Adaptation Strategy	791 Assign different blocks	792 Adjust sketch rank (sparsity)

## 793 C JUSTIFICATION FOR RANDOM- $k$ SKETCHING

794 FSLoRA is built upon Random- $k$  diagonal sketching due to two key properties:  
 795

- 796 • **Submatrix selection.** Given a sparse diagonal matrix  $\mathbf{S}_i$ , we have

$$797 \mathbf{BS}_i \mathbf{A} = \sum_{j \in \mathcal{I}_i} s_j \mathbf{b}_j \mathbf{a}_j^\top = [\mathbf{b}_j]_{j \in \mathcal{I}_i} \text{diag}\{s_j\}_{j \in \mathcal{I}_i} [\mathbf{a}_j^\top]_{j \in \mathcal{I}_i}, \quad (12)$$

798 where  $\mathcal{I}_i$  corresponds to the index set of non-zero diagonal entries of  $\mathbf{S}_i$  and  $\mathbf{b}_j$  and  $\mathbf{a}_j^\top$  denote  
 799 the  $j$ -th column of module  $\mathbf{B}$  and the  $j$ -th row of module  $\mathbf{A}$ , respectively. In other words, with  
 800 Random- $k$  sketching, only a subset of  $\mathbf{B}$ 's columns and  $\mathbf{A}$ 's rows are activated for client  $i$ . The  
 801 *sparse diagonal structure* effectively reduces local training cost for each client.  
 802

- 803 • **Unbiasedness for convergence.** When  $\mathbf{S}_i$  is a Random- $k$  diagonal matrix with  $k_i$  nonzero diagonal  
 804 entries  $s_j = \frac{r}{k_i}$ , we have

$$805 \mathbb{E}[\mathbf{BS}_i \mathbf{A}] = \mathbf{BA}. \quad (13)$$

806 This unbiasedness is critical for our convergence analysis.  
 807

808 Table C.1: Accuracy comparison of Random- $k$  sketching and importance-based sketching under the  
 809 commonsense reasoning benchmark with the LLaMA-3.2-3B model. Random- $k$  sketching achieves  
 810 better performance.  
 811

812 Importance metric	813 ARC-c	814 ARC-e	815 BoolQ	816 HSwag	817 OBQA	818 PIQA	819 SIQA	820 Wino	821 Avg.
817 $\ a\  \ b\ $	71.9	86.5	55.2	75.4	73.4	81.1	72.5	69.7	73.2
818 $\ a\  + \ b\ $	72.1	86.4	64.5	76.8	70.8	82.2	71.3	69.3	74.2
819 Random- $k$	75.8	86.7	69.7	81.4	80.4	83.9	76.2	78.8	79.1

In addition, we experimentally compare Random- $k$  sketching with importance-based sketching. For importance-based sketching, we sample (sketch)  $k_i$  components from  $\{\mathbf{b}_j \mathbf{a}_j^\top\}_{j=1}^r$  with probability set as the importance scores, e.g.,  $\|\mathbf{b}_j\|_2 + \|\mathbf{a}_j\|_2$  or spectral norm  $\|\mathbf{b}_j\|_2 \cdot \|\mathbf{a}_j\|_2$ . The results are shown in Table C.1. The results show that Random- $k$  diagonal sketching outperforms these choices for importance-based sketching. This may be because these importance measures are heuristic and do not reliably reflect actual contribution. Moreover, such sketching violates the unbiasedness property, complicating theoretical guarantees. While improved importance-based methods may enhance performance and remain a promising direction for future investigation, our current empirical and theoretical results favor random sketching.

## D COMPATIBILITY OF FSLoRA WITH SECURE AGGREGATION

The aggregation of FSLoRA is compatible with secure aggregation. Taking the aggregation of module **B** as an example, we illustrate this below.

In FSLoRA, client updates are sparse matrices with non-zero values only in columns indexed by  $\mathcal{I}_i \subset [r]$ , size  $|\mathcal{I}_i| = k_i$ . With secure aggregation, each client apply *additive masking*:

$$\tilde{\mathbf{B}}_i = \Delta\mathbf{B}_i + \mathbf{R}_i, \quad (14)$$

where mask  $\mathbf{R}_i$  satisfies  $\text{supp}(\mathbf{R}_i) \subseteq (u, v) : u \in [m], v \in \mathcal{I}_i$  and  $\sum_{i=1}^N \mathbf{R}_i = 0$ . That is, the mask has non-zero entries only in the client's active columns, and all masks together sum to zero to preserve correctness. Such masks can be constructed following the classical protocol: for each pair of clients  $(i, j)$ , define a random matrix

$$\mathbf{M}_{ij} = -\mathbf{M}_{ji} \in \mathbb{R}^{m \times r}, \quad \text{supp}(\mathbf{M}_{ij}) \subseteq (u, v) \mid u \in [m], v \in \mathcal{I}_i \cap \mathcal{I}_j, \quad (15)$$

and then construct its total mask

$$\mathbf{R}_i = \sum_{j>i} \mathbf{M}_{ij} - \sum_{j<i} \mathbf{M}_{ji}. \quad (16)$$

During uploading, client  $i$  sends the masked  $k_i$  non-zero columns of  $\tilde{\mathbf{B}}_i$ , and then the server adds the corresponding padding and averages them as:

$$\sum_{i=1}^N \tilde{\mathbf{B}}_i = \sum_{i=1}^N (\Delta\mathbf{B}_i + \mathbf{R}_i) = \sum_{i=1}^N \Delta\mathbf{B}_i, \quad (17)$$

which matches the aggregation of module **B** in (7). The aggregation of module **B** in FSLoRA is thus compatible with secure aggregation.

We can draw the same conclusion for module **A** under the same derivation.

## E EMPIRICAL VALIDATION OF ASSUMPTIONS

In the context of LLM fine-tuning, both the magnitude of stochastic gradients and gradients in LLM fine-tuning are in a mild range since:

- Transformer-based LLMs use *LayerNorm* and *scaled softmax attention*, which stabilize activations and suppress gradient spikes.
- Fine-tuning starts from a well-pretrained model already near a local minimum, leading to smaller gradients.
- The fine-tuning dataset does not typically contain strong contradictory signals to what the model already knows, resulting in a relatively flat loss surface.

To further support this empirically, we report the statistics of the expected norm of the stochastic gradients  $\mathbb{E}\|\nabla_{\mathbf{X}} \tilde{\ell}(\mathbf{X}, \xi; \mathbf{S})\|$  over approximately 4500 samples for 4 representative clients with different sketching ratios. The table below reports the minimum and maximum expected norm among 30 randomly sampled model states  $\mathbf{X} = [\mathbf{B}; \mathbf{A}]$ .

864  
865  
866 Table E.1: Statistics of the expected norm of stochastic gradients across clients.  
867  
868  
869  
870

Client ID	Number of samples	Rank	Min	Max
1	4580	4	0.1286	0.9499
2	4216	19	0.1284	0.7069
3	4873	9	0.1237	0.5774
4	5124	32	0.1499	0.8066

871  
872 As we can see from Table E.1, the expected norm, i.e.,  $\mathbb{E}_{\xi \sim \mathcal{D}_i, \mathbf{S} \sim \mathcal{S}_i} \|\nabla_{\mathbf{X}} \tilde{\ell}(\mathbf{X}, \xi; \mathbf{S})\|$ , is in a moderate  
873 range. Notably, the variance is upper-bounded by the expected squared gradient norm:  
874

$$875 \mathbb{E}_{\xi \sim \mathcal{D}_i, \mathbf{S} \sim \mathcal{S}_i} \|\nabla_{\mathbf{X}} \tilde{\ell}(\mathbf{X}, \xi; \mathbf{S}) - \nabla_{\mathbf{X}} f_i^S(\mathbf{X})\|^2 \leq \mathbb{E}_{\xi \sim \mathcal{D}_i, \mathbf{S} \sim \mathcal{S}_i} \|\nabla_{\mathbf{X}} \tilde{\ell}(\mathbf{X}, \xi; \mathbf{S})\|^2.$$

876 Therefore, it is generally not hard to find a  $\sigma$  and  $\rho$  to make Assumption 4.2 hold.  
877

878 On the other hand, we have  
879

$$\begin{aligned} & \|\nabla_{\mathbf{X}} f_i^S(\mathbf{X}) - \nabla_{\mathbf{X}} f^S(\mathbf{X})\|^2 \\ & \leq 2 \|\nabla_{\mathbf{X}} f_i^S(\mathbf{X})\|^2 + 2 \|\nabla_{\mathbf{X}} f^S(\mathbf{X})\|^2 \\ & \leq 2 \|\nabla_{\mathbf{X}} f_i^S(\mathbf{X})\|^2 + 2 \frac{1}{N} \sum_{i=1}^N \|\nabla_{\mathbf{X}} f_i^S(\mathbf{X})\|^2 \\ & \leq 2 \mathbb{E}_{\xi \sim \mathcal{D}_i, \mathbf{S} \sim \mathcal{S}_i} \|\nabla_{\mathbf{X}} \tilde{\ell}(\mathbf{X}, \xi; \mathbf{S})\|^2 + 2 \frac{1}{N} \sum_{i=1}^N \mathbb{E}_{\xi \sim \mathcal{D}_i, \mathbf{S} \sim \mathcal{S}_i} \|\nabla_{\mathbf{X}} \tilde{\ell}(\mathbf{X}, \xi; \mathbf{S})\|^2, \end{aligned} \quad (18)$$

888 where the first inequality follows Cauchy-Schwarz inequality, while the last inequality follows  
889 Jensen's inequality. Thus, the deviation can be controlled by the expected gradient norm, which we  
890 empirically found to be moderate (see Table E.1). Hence, it is reasonable to impose an upper bound  
891 on  $\|\nabla_{\mathbf{X}} f_i^S(\mathbf{X}) - \nabla_{\mathbf{X}} f^S(\mathbf{X})\|^2$  as in Assumption 4.3.  
892

## 893 F EVALUATION UNDER BROADER HETEROGENEITY AND INCREASED 894 NUMBER OF CLIENTS

895 To accommodate a larger number of clients, we extend FSLoRA (Algorithm 1) to support *partial*  
896 *client participation*. Specifically, at each round, the server samples a subset of clients, distributes  
897 the current global LoRA modules to them, and aggregates only the updates from these clients.  
898 Throughout this section, we fix the partial participation size to 10, i.e., 10 clients are sampled in each  
899 round.  
900

### 901 F.1 INCREASING RESOURCE HETEROGENEITY AND THE NUMBER OF CLIENTS

902 We extend our experiments on LLaMA-3.2-3B with the commonsense reasoning benchmark to 50  
903 clients. We adopt Dirichlet-based partitioning for dataset splits. Specifically, the commonsense  
904 reasoning benchmark includes 8 tasks, and we partitioned them based on the Dirichlet distribution  
905 to construct task heterogeneity among 50 clients. The Dirichlet concentration parameter is set to  
906  $\alpha = 0.1$ . We simulate client resource heterogeneity via different LoRA rank distributions (beyond  
907 the limited sketching ratio considered in Section 5). More capable clients are assigned higher ranks,  
908 reflecting varying compute capacities. We consider two different rank distributions: normal and  
909 heavy-tail distributions in the range [4, 64].  
910

911 **Normal distribution:** Ranks are sampled from a normal distribution with mean  $\mu = \frac{a+b}{2}$  and  
912 standard deviation  $\sigma = \frac{b-a}{6}$ , where  $a = 4$  and  $b = 64$ . This models a balanced distribution of client  
913 capabilities centered around the middle of the range.  
914

915 **Heavy-tail distribution:** We sample ranks using an inverse log-normal distribution. Specifically,  
916 we draw  $x_i \sim \text{LogNormal}(\mu, \sigma)$  with  $\mu = \log(\frac{a+b}{4})$  and  $\sigma = 1.0$ , then set  $k_i = 1/x_i$  and apply  
917 min-max normalization to scale values into the range  $[a, b]$ . This results in a heavy-tailed distribution  
918

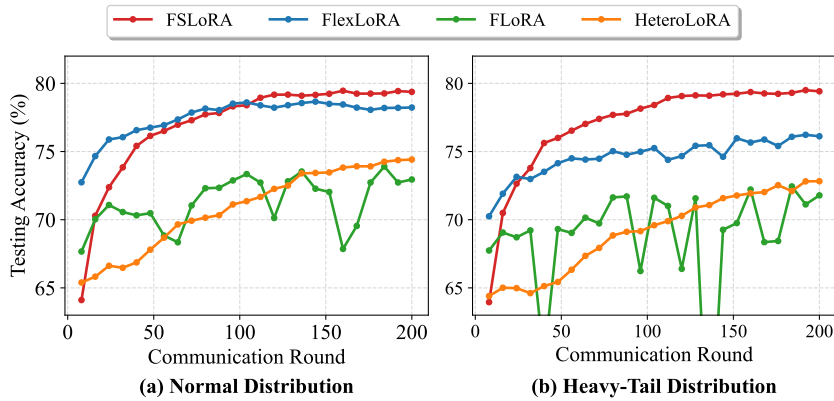
918 where most clients receive low ranks, reflecting a scenario with many low-capability clients and a  
 919 few high-capability ones.  
 920

921 Table F.1: Accuracy comparison under different client heterogeneity settings. FSLoRA outperforms  
 922 baseline methods across both normal and heavy-tail LoRA rank distributions.  
 923

Rank setup	Method	ARC-c	ARC-e	BoolQ	HellaSwag	OBQA	PIQA	SIQA	WinoGrande	Avg.
Normal	HeteroLoRA	73.38	85.82	62.17	71.23	77.40	80.14	74.72	72.53	74.67
	FlexLoRA	74.23	87.84	68.37	79.77	76.00	82.97	75.90	78.13	77.90
	FLoRA	68.17	83.75	64.93	75.67	71.40	77.20	71.24	70.09	72.81
	FSLoRA	75.77	86.95	69.67	81.53	80.60	84.06	76.20	78.85	79.20
Heavy-tail	HeteroLoRA	72.44	86.78	63.60	73.10	72.00	81.34	71.65	68.75	73.71
	FlexLoRA	73.04	86.70	62.23	75.57	78.00	81.12	74.77	73.32	75.59
	FLoRA	67.92	81.90	64.90	72.77	74.00	80.41	75.28	70.24	73.43
	FSLoRA	75.77	86.70	69.67	81.40	80.40	83.90	76.15	78.77	79.10

932  
 933 As shown in Table F.1, FSLoRA outperforms other methods under both heterogeneity settings. As we  
 934 move from normal to heavy-tail, where more clients are low-resource, overall performance decreases  
 935 for all methods. However, FSLoRA exhibits the smallest drop, demonstrating stronger robustness to  
 936 extreme client heterogeneity.

937 In Figure 4, we compare the convergence behavior of FSLoRA and three baseline methods under the  
 938 aforementioned two types of client heterogeneity. Under the normal distribution, FlexLoRA exhibits  
 939 fast initial progress but falls behind FSLoRA in final accuracy, likely due to approximation errors  
 940 introduced by truncated SVD. This issue is exacerbated in the heavy-tail distribution, where low-rank  
 941 clients dominate and SVD truncation causes greater distortion, further degrading FlexLoRA’s perfor-  
 942 mance. Similarly, HeteroLoRA’s reliance on zero-padding reduces optimization efficiency, preventing  
 943 it from achieving higher accuracy. FLoRA fails to show steady improvement as communication  
 944 progresses. One potential reason is that frequent model merging and random reinitialization of LoRA  
 945 modules in each round disrupt the convergence continuity. In contrast, FSLoRA demonstrates robust  
 946 and stable convergence across both scenarios, achieving the highest overall accuracy.



950 Figure 4: Convergence behavior of FSLoRA and baselines on the commonsense reasoning benchmark  
 951 with the LLaMA-3.2-3B model. Notably, FSLoRA’s per-round communication cost is at most equal  
 952 to the baselines (as detailed in Appendix A). Testing accuracy is averaged over eight tasks.  
 953

## 954 F.2 FURTHER INCREASING THE NUMBER OF CLIENTS

955  
 956 We further evaluated the performance of FSLoRA by increasing the number of clients to 100. The  
 957 results are presented in Table F.2. In this setting, local ranks follow a heavy-tailed distribution as  
 958 described in the previous subsection, and all other experimental configurations remain unchanged.  
 959 As shown in the table, FSLoRA maintains its advantage in terms of the average performance when  
 960 scaling to more clients.

972 Table F.2: Accuracy comparison when the number of clients is  $N = 100$ . FSLoRA maintains its  
 973 advantage in terms of the average accuracy.  
 974

Method	ARC-c	ARC-e	BoolQ	HellaSwag	OBQA	PIQA	SIQA	WinoGrande	Avg.
HeteroLoRA	71.76	86.24	62.57	68.07	76.60	79.38	74.10	69.69	73.55
FlexLoRA	73.38	87.54	69.03	75.27	78.60	80.47	74.16	73.80	76.53
FLoRA	69.97	83.25	67.10	71.67	73.60	78.94	72.21	70.80	73.44
<b>FSLoRA</b>	<b>74.40</b>	<b>87.54</b>	<b>70.13</b>	<b>79.90</b>	<b>79.40</b>	<b>83.57</b>	<b>76.51</b>	<b>78.93</b>	<b>78.80</b>

### 980 981 F.3 VARYING THE LEVEL OF DATA HETEROGENEITY 982

983 In Table F.3, we investigate the impact of the degree of data heterogeneity on performance. We  
 984 increase the heterogeneity by decreasing the Dirichlet concentration parameter from  $\alpha = 1$  to  
 985  $\alpha = 0.1$ . The local ranks follow the heavy-tail distribution described in the previous subsection,  
 986 and all other experimental configurations remain consistent with Appendix F.1. As observed from  
 987 Table F.3, the performance of all methods degrades as heterogeneity increases. FSLoRA consistently  
 988 achieves higher accuracy.  
 989

990 Table F.3: Accuracy comparison under different data heterogeneity settings. FSLoRA maintains its  
 991 advantage over the baselines as the data heterogeneity increases. The number of clients is set to 50.  
 992

Data setup	Method	ARC-c	ARC-e	BoolQ	HellaSwag	OBQA	PIQA	SIQA	WinoGrande	Avg.
Dir(1)	HeteroLoRA	72.18	86.11	62.57	73.10	77.60	79.82	74.26	69.46	74.39
	FlexLoRA	74.06	87.25	65.67	74.90	78.80	81.01	74.16	74.27	76.27
	FLoRA	70.14	83.29	67.27	71.60	73.60	78.73	72.16	70.96	73.47
	<b>FSLoRA</b>	<b>75.85</b>	<b>87.50</b>	<b>70.93</b>	<b>81.47</b>	<b>81.00</b>	<b>82.86</b>	<b>76.66</b>	<b>78.53</b>	<b>79.35</b>
Dir(0.1)	HeteroLoRA	72.44	86.78	63.60	73.10	72.00	81.34	71.65	68.75	73.71
	FlexLoRA	73.04	86.70	62.23	75.57	78.00	81.12	74.77	73.32	75.59
	FLoRA	67.92	81.90	64.90	72.77	74.00	80.41	75.28	70.24	73.43
	<b>FSLoRA</b>	<b>75.77</b>	<b>86.70</b>	<b>69.67</b>	<b>81.40</b>	<b>80.40</b>	<b>83.90</b>	<b>76.15</b>	<b>78.77</b>	<b>79.10</b>

## 1000 1001 G EXPERIMENTS ON QWEN2.5-1.5B-INSTRUCT AND LLAMA-7B 1002

1004 We further extended our evaluation to the Qwen model. Specifically, we fine-tuned Qwen2.5-1.5B-  
 1005 Instruct on the commonsense reasoning benchmark using the same setup as in Table 5.1. As shown  
 1006 in Table G.1, FSLoRA achieves competitive performance compared with the heterogeneous LoRA  
 1007 baselines, suggesting its effective across different model architectures.  
 1008

1009 Table G.1: Performance comparison with Qwen2.5-1.5B-Instruct. FSLoRA maintains its advantage.  
 1010

Method	ARC-c	ARC-e	BoolQ	HellaSwag	OBQA	PIQA	SIQA	WinoGrande	Avg.
HeteroLoRA	70.36	86.53	65.50	68.55	79.01	74.93	68.25	68.04	72.65
FlexLoRA	73.41	88.07	63.32	71.30	76.44	78.02	70.94	68.56	73.76
FLoRA	70.28	84.51	60.90	68.82	69.58	73.45	67.53	66.27	70.17
<b>FSLoRA</b>	<b>75.82</b>	<b>88.16</b>	<b>65.08</b>	<b>74.93</b>	<b>79.82</b>	<b>80.72</b>	<b>72.62</b>	<b>71.29</b>	<b>76.06</b>

1016  
 1017 Although our primary focus is on models suitable for client-side deployment, such as RoBERTa and  
 1018 LLaMA-3.2-3B models, we also include experiments on the larger LLaMA-7B model to demonstrate  
 1019 the scalability of FSLoRA in more complex models. Specifically, we fine-tune the LLaMA-7B  
 1020 model on the Wizard, Dolly-15k, and Alpaca datasets and evaluate it on 1444 MMLU samples  
 1021 (available at: <https://github.com/ATP-1010/FederatedLLM>). For Wizard and Dolly-15k, we adopt  
 1022 the same heterogeneous data partitioning as (Wang et al., 2024). Since the Alpaca dataset lacks  
 1023 a clear task or domain structure, we apply a uniform random partitioning strategy to distribute  
 1024 the data across clients. We tune the q-proj and v-proj modules and set the local LORA ranks  
 1025  $k_i = [64, 32, 16, 16, 8, 8, 4, 4, 4, 4]$  for 10 clients. The parameter settings are aligned with those in  
 (Wang et al., 2024).

1026  
1027  
1028 Table G.2: Performance comparison on LLaMA-7B model.  
1029  
1030  
1031  
1032  
1033

Method	Wizard	Dolly-15k	Alpaca	Avg
HeteroLoRA	27.15	26.70	28.74	27.53
FlexLoRA	28.25	35.60	30.40	31.42
FLoRA	27.91	28.50	29.54	28.65
<b>FSLoRA</b>	<b>30.33</b>	<b>40.79</b>	<b>30.68</b>	<b>33.93</b>

1034  
1035  
1036 As shown in Table G.2, FSLoRA achieves the highest average performance across all three datasets  
1037 compared to baselines. These results demonstrate FSLoRA’s potential for effective fine-tuning with  
1038 the large-scale LLaMA-7B model under heterogeneous client settings.

## 1040 H FURTHER EXPERIMENTS

1041  
1042  
1043 In this section, we provide additional results, including detailed per-task comparisons from the  
1044 commonsense reasoning benchmark corresponding to Figures 3(a) and 3(b). In addition, we further  
1045 investigate the impact of the number of local updates  $H$  on the convergence, the robustness of  
1046 FSLoRA under dynamic sketching ratio, and the integration of communication compression and  
1047 sketching.

### 1048 H.1 FURTHER DETAILS ON THE ABLATION STUDY

1049  
1050  
1051 **Impact of sketching:** In Figure 5, we compare the performance of FSLoRA with and without  
1052 sketching on eight tasks from the commonsense reasoning benchmark using the LLaMA-3.2-3B  
1053 model. Notably, FSLoRA without sketching is equivalent to the vanilla Federated LoRA. For  
1054 FSLoRA with sketching, we apply a uniform sketching ratio of  $k_i/r = 0.5$  across all distributed  
1055 clients. The uploading budget for each client is set to 200 times the size of the full global LoRA  
1056 modules at the corresponding rank. It is clear that FSLoRA with sketching consistently outperforms  
1057 its non-sketched counterpart across these eight tasks, demonstrating the effectiveness of sketching in  
1058 improving performance.

1059  
1060  
1061 **Impact of the global rank:** In Figure 6, we present the impact of the rank of the global LoRA modules  
1062 on FSLoRA’s performance across eight tasks from the commonsense reasoning benchmark. We  
1063 consider four configurations: 1)  $r = 8$ ,  $k_i/r = 1$ , 2)  $r = 16$ ,  $k_i/r = 0.5$ , 3)  $r = 32$ ,  $k_i/r = 0.25$ ,  
1064 and 4)  $r = 64$ ,  $k_i/r = 0.125$ . The rank of submatrices updated by the clients at each iteration remains  
1065 consistent across all configurations (i.e.,  $k_i = 8$ ), ensuring that the communication and computational  
1066 resources on the client side are kept fixed for all cases. In the ARC-Easy task, performance decreases  
1067 as the rank increases to 64, potentially due to overfitting. In general, FSLoRA shows improved  
1068 performance as the rank increases.

### 1069 H.2 IMPACT OF LOCAL UPDATES

1070  
1071 Based on the commonsense reasoning benchmark and the LLaMA-3.2-3B model, we evaluated  
1072 the convergence behavior of FSLoRA under varying numbers of local updates (i.e.,  $H$ ). The  
1073 experimental results are presented in Figure 7. In the low-to-moderate regime of local updates (i.e.,  
1074  $H \in 10, 20, 100$ ), FSLoRA demonstrates a clear acceleration in convergence as  $H$  increases. For  
1075 example, moving from  $H = 10$  to  $H = 20$  substantially reduces the number of communication  
1076 rounds required to reach the same level of testing accuracy, while further increasing  $H$  to 100 yields  
1077 even faster progress toward convergence. This observation indicates that a moderate increase in local  
1078 updates allows clients to improve communication efficiency. However, when the number of local  
1079 updates is pushed beyond this range (e.g.,  $H = 200$ ), no additional convergence gain is observed.  
These findings align well with our theoretical analysis in Section 4, which shows that FSLoRA can  
achieve a convergence speedup under certain conditions on  $H$ .

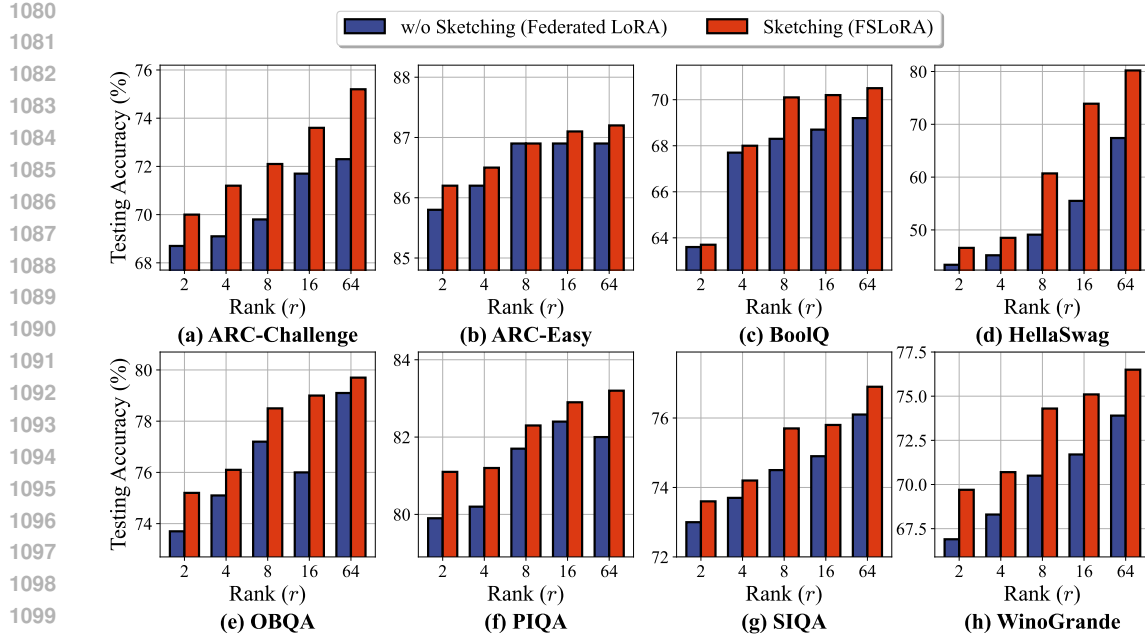


Figure 5: Comparison of FSLoRA with and without sketching, with an upload budget  $200 \times$  the global LoRA module size at each rank. This is based on the commonsense reasoning benchmark and the LLaMA-3.2-3B model. We observe that the sketching mechanism improves performance across all considered tasks. The average accuracy of the eight tasks is shown in Figure 3(a).

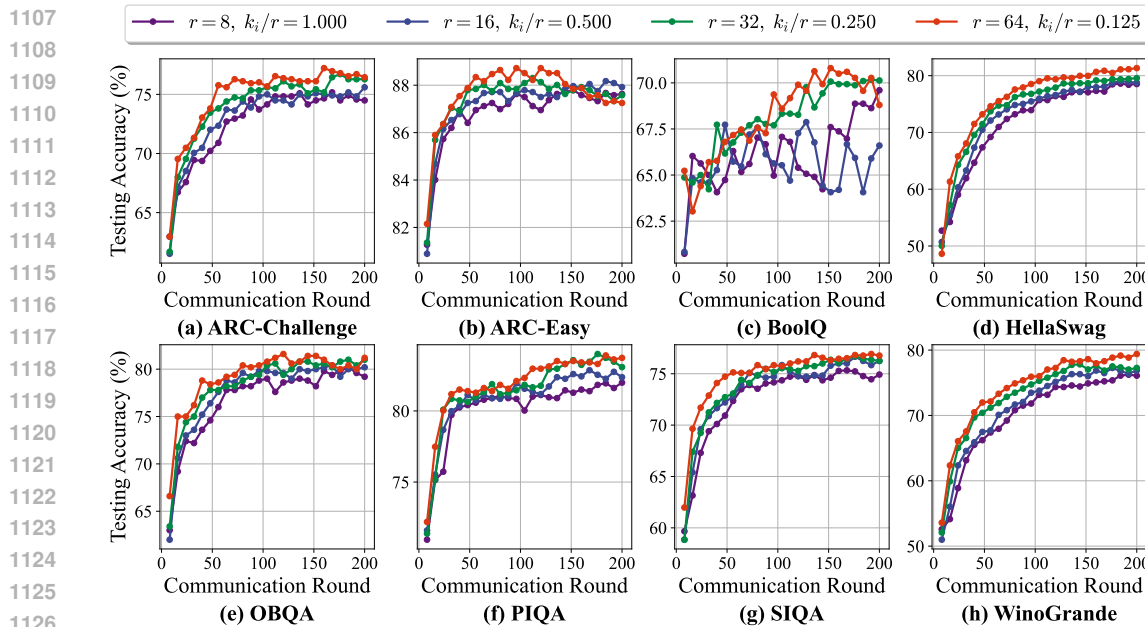


Figure 6: Impact of the rank of global LoRA modules on FSLoRA, given a fixed rank for the updated submatrices at the clients. This is based on the commonsense reasoning benchmark and the LLaMA-3.2-3B model. Overall, FSLoRA demonstrates improved performance as the global rank increases. The average accuracy of the eight tasks is shown in Figure 3(b).

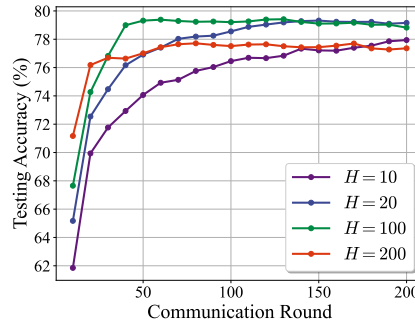


Figure 7: Impact of the number of local updates on FSLoRA’s convergence. This is based on the commonsense reasoning benchmark and the LLaMA-3.2-3B model. In a certain range, i.e., from 10 to 100, FSLoRA achieves a fast convergence as  $H$  increases.

### H.3 DYNAMIC SKETCHING RATIOS

While our primary focus is on developing a heterogeneous federated LoRA method under a standard static setup, following prior works (Wang et al., 2024; Cho et al., 2024; Bai et al., 2024), the proposed FSLoRA algorithm can be naturally extended to dynamic, time-varying resource environments. The modification is straightforward: we allow the sparsity levels, corresponding to the sketching ratios of FSLoRA, of the matrices in the sketching set  $\mathcal{S}_i$  in Algorithm 1 to become time-varying, while keeping the remaining steps unchanged.

We empirically validate the effectiveness of FLoRA under this dynamic setting. In the simulation, we group clients into three capability levels *low*, *medium*, and *high*, assigned sketching ratio ranges  $[0.125, 0.25]$ ,  $[0.25, 0.5]$ , and  $[0.5, 1.0]$ , respectively, to balance local training latencies across groups. Within each range, the sketching ratios are allowed to vary dynamically. The results, reported in Table H.1, show that FSLoRA maintains comparable performance when moving from the static to the dynamic case, demonstrating its robustness under time-varying sketching ratios.

Table H.1: The performance of FSLoRA under static and dynamic sketching ratios. This is based on the commonsense reasoning benchmark and the LLaMA-3.2-3B model. FSLoRA maintains comparable performance when moving from the static to the dynamic case.

Ratios	ARC-c	ARC-e	BoolQ	HSwag	OBQA	PIQA	SIQA	Wino	Avg.
Static	76.1	87.1	70.0	81.7	81.4	82.6	76.4	78.9	79.3
Dynamic	75.5	87.7	69.2	81.3	81.2	82.2	76.0	78.8	79.0

### H.4 INTEGRATION OF SKETCHING AND TOP-K COMPRESSION

Building on the commonsense reasoning benchmark and the LLaMA-3.2-3B model, we further explore the integration of two orthogonal techniques, sketching and top-k compression, to further reduce the uplink communication overhead of clients in FSLoRA.

Specifically, with sketching, each client activates and updates submatrices of the global LoRA weights,  $[\mathbf{b}_j]_{j \in \mathcal{I}_i}, [\mathbf{a}_j^\top]_{j \in \mathcal{I}_i}$ , which are selected at the beginning of each round:

$$\mathbf{B}\mathbf{S}_i\mathbf{A} = \sum_{j \in \mathcal{I}_i} \frac{r}{k_i} \mathbf{b}_j \mathbf{a}_j^\top = \frac{r}{k_i} [\mathbf{b}_j]_{j \in \mathcal{I}_i} [\mathbf{a}_j^\top]_{j \in \mathcal{I}_i}, \quad (19)$$

where  $\mathbf{b}_j$  and  $\mathbf{a}_j^\top$  denote the  $j$ -th column of module  $\mathbf{B}$  and the  $j$ -th row of module  $\mathbf{A}$ , respectively. By limiting updates to submatrices  $[\mathbf{b}_j]_{j \in \mathcal{I}_i}$  and  $[\mathbf{a}_j^\top]_{j \in \mathcal{I}_i}$ , FSLoRA reduces communication and computation. To further reduce communication cost, we can apply Top- $k$  compression to the uploading stage. For instance, instead of sending the full  $\Delta[\mathbf{b}_j]_{j \in \mathcal{I}_i}$ , each client transmits the compressed update  $\text{Top}_k(\Delta[\mathbf{b}_j]_{j \in \mathcal{I}_i})$ . Sketching selects the update submatrix at the beginning of

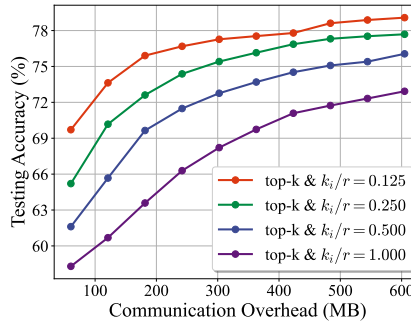


Figure 8: Testing accuracy versus communication overhead using float 32 precision. Lower sketching ratios achieve higher accuracy at the same communication cost, demonstrating that combining sketching with top- $k$  compression leads to more communication-efficient training.

each round, while compression further reduces its transmission cost at the uploading stage. These two techniques operate at different stages and can jointly improve communication efficiency.

In our setup, the compression ratio is fixed at 0.5 for all methods, while the sketching ratio  $k_i/r$  varies over  $\{0.125, 0.25, 0.5, 1\}$ . Notably, FSLoRA with sketching ratio  $k_i/r = 1$  corresponds to the vanilla Federated LoRA (i.e., without sketching). Figure 8 plots testing accuracy versus communication overhead, where the x-axis represents the amount of data uploaded per client (in MB), assuming parameters are stored in float 32 precision. The results clearly show that integrating sketching with top- $k$  compression further improves communication efficiency: methods with lower sketching ratios consistently achieve higher accuracy under the same communication budget, highlighting the potential of FSLoRA for scalable and communication-efficient collaborative LLM fine-tuning.

## I IMPLEMENTATION DETAILS

### I.1 DETAILS ON HYPERPARAMETERS

Unless stated otherwise, the hyperparameters used in this work are as follows.

Table I.1: The hyperparameters for RoBERTa & GLUE and LLaMA-3.2-3B & commonsense reasoning benchmarks.

Hyperparameter	RoBERTa & GLUE	LLaMA-3.2-3B & commonsense reasoning
Dirichlet parameter	0.1	0.1
Batch size	16	16
LoRA dropout rate	0.1	0.1
Learning rate, $\gamma$	5e-4	3e-4
Communication round, $T$	200	200
Local iteration number, $H$	50	20
Target module	["query", "value", "classification head"]	["q-proj", "k-proj", "v-proj", "up-proj", "down-proj"]

### I.2 DETAILS ON DATASETS

#### I.2.1 GLUE BENCHMARK

GLUE is a widely recognized benchmark designed to assess the natural language understanding capabilities of language models (Wang, 2018).

- **CoLA** focuses on whether a given sentence is acceptable according to linguistic rules. It evaluates a model’s ability to recognize well-formed sentences.

▷ Input: A single sentence.

☆ Output: A label indicating whether the sentence is acceptable or unacceptable.

- 1242 • **SST-2** is designed for sentiment classification on movie reviews or short texts. It tests whether a  
 1243 model can correctly identify positive or negative sentiment in a given sentence.  
 1244
  - ▷ Input: A single sentence.
  - ☆ Output: A label indicating positive or negative sentiment.
- 1245 • **MRPC** checks if two sentences are paraphrases of each other, i.e., if they mean the same thing.  
 1246
  - ▷ Input: Two sentences ('sentence1' and 'sentence2').
  - ☆ Output: A label indicating either equivalent or not equivalent.
- 1247 • **QQP** tests a model's ability to determine if two questions ask the same thing.  
 1248
  - ▷ Input: Two questions.
  - ☆ Output: A label indicating duplicate or not duplicate.
- 1249 • **MNLI** tests whether a given hypothesis is entailed, contradicted, or neutral with respect to a  
 1250 premise.  
 1251
  - ▷ Input: A premise (first sentence) and a hypothesis (second sentence).
  - ☆ Output: A label indicating entailment, contradiction, or neutral.
- 1252 • **QNLI** aims to determine if a context sentence correctly answers a given question.  
 1253
  - ▷ Input: A question and a sentence.
  - ☆ Output: A label indicating the sentence answers the question or it does not.
- 1254 • **RTE** provides pairs of sentences to see if one implies the other.  
 1255
  - ▷ Input: Two sentences ('sentence1' and 'sentence2')
  - ☆ Output: A label indicating whether the meaning of one sentence is entailed from the other one.

### 1269 I.2.2 COMMONSENSE REASONING BENCHMARK

1270 The training set of the commonsense reasoning benchmark is a mixture of multiple datasets including  
 1271 about 170K training samples from ARC-c/e (Clark et al., 2018), BoolQ (Clark et al., 2019), HellaSwag  
 1272 (Zellers et al., 2019), OBQA (Mihaylov et al., 2018), PIQA (Bisk et al., 2020), SIQA (Sap et al.,  
 1273 2019), and WinoGrande (Sakaguchi et al., 2021) datasets.

- 1274 • **ARC-c/e** contains the challenge and easy question set from the ARC dataset of genuine grade-school  
 1275 level, multiple-choice science questions.
- 1276 • **BoolQ** is a question-answering dataset with yes/no questions derived from natural, real-world  
 1277 scenarios.
- 1278 • **HellaSwag** includes questions for commonsense natural language inference, where a context and  
 1279 multiple endings are given, requiring the most coherent ending to be selected.
- 1280 • **OBQA** involves multi-step problem-solving that combines commonsense knowledge, reasoning,  
 1281 and comprehension of accompanying textual information.
- 1282 • **PIQA** focuses on questions requiring physical commonsense to solve. Each question offers two  
 1283 answer choices.
- 1284 • **SIQA** targets reasoning about human actions and their social implication.
- 1285 • **WinoGrande** is designed as a binary-choice fill-in-the-blank task, this dataset evaluates the ability  
 1286 to resolve ambiguous sentences through commonsense reasoning.

1287 The input template, i.e., prompt format for these datasets is detailed in Table I.2.

1296 Table I.2: The prompt template of the commonsense reasoning datasets (Hu et al., 2023).  
1297

1298 Dataset	1299 Input Template
1300	Please choose the correct answer to the question: [QUESTION]
1301	Answer1: [ANSWER_1]
1302	Answer2: [ANSWER_2]
1303	Answer3: [ANSWER_3]
1304	Answer4: [ANSWER_4]
1305	Answer format: answer1/answer2/answer3/answer4
1306	the correct answer is [ANSWER]
1307	
1308	Please answer the following question with true or false, question: [QUES-]
1309	TION]
1310	Answer format: true/false
1311	the correct answer is [ANSWER]
1312	
1313	Please choose the correct ending to complete the given sentence: [ACTIV-]
1314	ITY_LABEL]: [CONTEXT]
1315	Ending1: [ENDING_1]
1316	Ending2: [ENDING_2]
1317	Ending3: [ENDING_3]
1318	Ending4: [ENDING_4]
1319	Answer format: ending1/ending2/ending3/ending4
1320	the correct answer is [ANSWER]
1321	
1322	Please choose the correct answer to the question: [QUESTION]
1323	Answer1: [ANSWER_1]
1324	Answer2: [ANSWER_2]
1325	Answer3: [ANSWER_3]
1326	Answer4: [ANSWER_4]
1327	Answer format: answer1/answer2/answer3/answer4
1328	the correct answer is [ANSWER]
1329	
1330	Please choose the correct solution to the question: [QUESTION]
1331	Solution1: [SOLUTION_1]
1332	Solution2: [SOLUTION_2]
1333	Answer format: solution1/solution2
1334	the correct answer is [ANSWER]
1335	
1336	Please choose the correct answer to the question: [QUESTION]
1337	Answer1: [ANSWER_1]
1338	Answer2: [ANSWER_2]
1339	Answer3: [ANSWER_3]
1340	Answer format: answer1/answer2/answer3
1341	the correct answer is [ANSWER]
1342	
1343	Please choose the correct answer to fill in the blank to complete the given
1344	sentence: [SENTENCE]
1345	Option1: [OPTION_1]
1346	Option2: [OPTION_2]
1347	the correct answer is [ANSWER]
1348	
1349	

1350 **J PROOF OF THE THEORETICAL RESULTS**

1351 **J.1 PRELIMINARIES**

1352 Before presenting the proof of the main results, we first introduce some preliminary facts that will be  
 1353 used later. Throughout this work,  $\|\cdot\|$  denotes the Frobenius norm when applied to a matrix and the  
 1354  $\ell_2$  norm when applied to a vector.

1355 **Lemma J.1.** *Suppose a sequence of independent random matrices  $\{\mathbf{P}_i\}_{i=1}^N$  satisfy  $\mathbb{E}[\mathbf{P}_i] = \mathbf{0}, \forall i$ . Then,*

$$1356 \mathbb{E} \left\| \frac{1}{N} \sum_{i=1}^N \mathbf{P}_i \right\|^2 = \frac{1}{N^2} \sum_{i=1}^N \mathbb{E} \|\mathbf{P}_i\|^2. \quad (20)$$

1357 **Lemma J.2.** (Wang et al., 2021, Lemma 2) *Suppose a sequence of random matrices  $\{\mathbf{P}_i\}_{i=1}^N$  satisfy  
 1358  $\mathbb{E}[\mathbf{P}_i | \mathbf{P}_{i-1}, \mathbf{P}_{i-2}, \dots, \mathbf{P}_1] = \mathbf{0}, \forall i$ . Then,*

$$1359 \mathbb{E} \left[ \left\| \sum_{i=1}^N \mathbf{P}_i \right\|^2 \right] = \sum_{i=1}^N \mathbb{E} [\|\mathbf{P}_i\|^2]. \quad (21)$$

1360 **Lemma J.3.** (Koloskova et al., 2020, Lemma 17) *For any  $a_0 \geq 0, b \geq 0, c \geq 0, d > 0$ , there exist a  
 1361 constant  $\eta \leq \frac{1}{d}$  such that*

$$1362 \frac{a_0}{T\eta} + b\eta + c\eta^2 \leq 2 \left( \frac{a_0 b}{T} \right)^{\frac{1}{2}} + 2c^{\frac{1}{3}} \left( \frac{a_0}{T} \right)^{\frac{2}{3}} + \frac{d a_0}{T}. \quad (22)$$

1363 **Lemma J.4** (Random sketching bounds). *Let  $\mathbf{S}$  be a random diagonal sketching matrix of the form*

$$1364 \mathbf{S} = \frac{r}{k} \sum_{j \in \mathcal{I}} \mathbf{e}_j \mathbf{e}_j^\top, \quad (23)$$

1365 where  $\mathbf{e}_1, \dots, \mathbf{e}_r \in \mathbb{R}^r$  are standard unit basis vectors and  $\mathcal{I} \subseteq \{1, \dots, r\}$  is chosen uniformly at  
 1366 random with  $|\mathcal{I}| = k$ . Then any matrix  $\mathbf{X}$  we have

$$1367 \|\mathbf{X} \mathbf{S}\|^2 \leq \frac{r^2}{k^2} \|\mathbf{X}\|^2, \quad (24)$$

1368 and in expectation we have

$$1369 \mathbb{E}_{\mathbf{S}} [\|\mathbf{X} \mathbf{S}\|^2] \leq \frac{r}{k} \|\mathbf{X}\|^2. \quad (25)$$

1370 *Proof.* Since  $\mathbf{S}$  is diagonal with exactly  $k$  diagonal entries equal to  $\frac{r}{k}$  and the rest zero, its largest  
 1371 eigenvalue is  $\frac{r}{k}$ . Squaring gives

$$1372 \mathbf{S} \mathbf{S}^\top = \mathbf{S}^2 \preceq \frac{r^2}{k^2} \mathbf{I}, \quad (26)$$

1373 Equivalently,

$$1374 \mathbf{x}^\top (\mathbf{S} \mathbf{S}^\top) \mathbf{x} \leq \frac{r^2}{k^2} \|\mathbf{x}\|^2, \forall \mathbf{x}. \quad (27)$$

1375 Setting  $\mathbf{x} = \mathbf{x}_j$  to be the  $j$ -th column of  $\mathbf{X}$  and summing over  $j$  implies

$$1376 \|\mathbf{X} \mathbf{S}\|^2 = \sum_j \|\mathbf{S}^\top \mathbf{x}_j\|^2 = \sum_j \mathbf{x}_j^\top (\mathbf{S} \mathbf{S}^\top) \mathbf{x}_j \leq \frac{r^2}{k^2} \sum_j \|\mathbf{x}_j\|^2 = \frac{r^2}{k^2} \|\mathbf{X}\|^2, \quad (28)$$

1377 which proves (24).

1378 For the expected bound (25), note that each diagonal index  $j \in \{1, \dots, r\}$  is included in  $\mathcal{I}$  with  
 1379 probability  $\frac{k}{r}$ . Hence the expectation of  $\mathbf{S}^2$  satisfies

$$1380 \mathbb{E}_{\mathbf{S}} [\mathbf{S}^2] = \frac{r^2}{k^2} \mathbb{E} \left[ \sum_{j \in \mathcal{I}} \mathbf{e}_j \mathbf{e}_j^\top \right] = \frac{r^2}{k^2} \frac{k}{r} \mathbf{I} = \frac{r}{k} \mathbf{I}. \quad (29)$$

1404 Thus for any vector  $\mathbf{x}$ ,

$$1406 \mathbb{E}_{\mathbf{S}}[\|\mathbf{S}^\top \mathbf{x}\|^2] = \mathbb{E}_{\mathbf{S}}[\mathbf{x}^\top \mathbf{S} \mathbf{S}^\top \mathbf{x}] = \mathbf{x}^\top (\mathbb{E}[\mathbf{S}^2]) \mathbf{x} = \frac{r}{k} \|\mathbf{x}\|^2. \quad (30)$$

1408 Summing over columns of  $\mathbf{X}$  again establishes

$$1410 \mathbb{E}_{\mathbf{S}}[\|\mathbf{X} \mathbf{S}\|^2] = \sum_j \mathbb{E}_{\mathbf{S}}[\|\mathbf{S}^\top \mathbf{x}_j\|^2] = \sum_j \mathbf{x}_j^\top (\mathbb{E}[\mathbf{S}^2]) \mathbf{x}_j = \frac{r}{k} \|\mathbf{X}\|^2. \quad (31)$$

1413 This completes the proof of Lemma J.4.  $\square$

## 1415 J.2 PROOF OF LEMMA 3.2

1417 From the chain rule for matrix calculus, we know that:

$$1419 \nabla_{\mathbf{Y}} g(\mathbf{XY}) = \mathbf{X}^\top \nabla g(\mathbf{XY}), \nabla_{\mathbf{X}} g(\mathbf{XY}) = \nabla g(\mathbf{XY}) \mathbf{Y}^\top, \quad (32)$$

1421 where  $\nabla g(\mathbf{XY})$  denotes the gradient of  $g$  to  $\mathbf{XY}$ . Applying this to  $\ell(\mathbf{W}_0 + \mathbf{BSA}, \xi)$ , we proceed as follows:

1423 To compute the gradient with respect to  $\mathbf{B}$ , set  $\mathbf{X} = \mathbf{B}$  and  $\mathbf{Y} = \mathbf{SA}$ :

$$1424 \nabla_{\mathbf{B}} \ell(\mathbf{W}_0 + \mathbf{BSA}, \xi) = \nabla \ell(\mathbf{W}_0 + \mathbf{BSA}, \xi) (\mathbf{SA})^\top. \quad (33)$$

1426 Similarly, to compute the gradient with respect to  $\mathbf{A}$ , set  $\mathbf{X} = \mathbf{BS}$  and  $\mathbf{Y} = \mathbf{A}$ :

$$1428 \nabla_{\mathbf{A}} \ell(\mathbf{W}_0 + \mathbf{BSA}, \xi) = \mathbf{S}^\top \mathbf{B}^\top \nabla \ell(\mathbf{W}_0 + \mathbf{BSA}, \xi). \quad (34)$$

## 1430 J.3 PROOF OF THEOREM 4.4

1432 The proof of Theorem 4.4 relies on the following proposition.

1434 **Proposition J.5.** *Under Assumption 4.1,  $\tilde{f}_i(\mathbf{X}; \mathbf{S}) = f_i(\mathbf{BS}, \mathbf{A})$ ,  $\mathbf{S} \in \mathcal{S}_i$ ,  $f_i^S(\mathbf{X}) = \mathbb{E}_{\mathbf{S} \sim \mathcal{S}_i}[\tilde{f}_i(\mathbf{X}; \mathbf{S})]$ , and  $f^S(\mathbf{X}) = \frac{1}{N} \sum_{i=1}^N f_i^S(\mathbf{X})$  are smooth with parameters  $L \frac{r^2}{k_i^2}$ ,  $L \frac{r}{k_i}$ , and  $\left(\frac{1}{N} \sum_{i=1}^N \frac{r}{k_i}\right) L$ , respectively.*

1438 The proof of Proposition J.5 is deferred to Appendix J.4. With this proposition, we are ready to prove Theorem 4.4.

1441 In FSLoRA, the update direction in (5) corresponds to the negative stochastic gradient of  $\ell(\mathbf{W}_0 +$   
1442  $\mathbf{BSA}, \xi)$  with respect to  $[\mathbf{B}; \mathbf{A}]$  for a given sketch  $\mathbf{S}_i^t$ . We have defined  $\tilde{\ell}(\mathbf{X}, \xi; \mathbf{S}) = \ell(\mathbf{W}_0 +$   
1443  $\mathbf{BSA}, \xi)$ . The iterative equation for the proposed FSLoRA algorithm thus can be written as

$$1445 \mathbf{X}^{t+1} = \mathbf{X}^t - \gamma \frac{1}{N} \sum_{i=1}^N \sum_{h=0}^{H-1} \nabla_{\mathbf{X}} \tilde{\ell}(\mathbf{X}_i^{t,h}, \xi_i^{t,h}; \mathbf{S}_i^t), \quad (35)$$

1448 where  $\mathbf{g}_i^{t,h}$  denotes the stochastic gradient  $\nabla_{\mathbf{X}} \tilde{\ell}(\mathbf{X}_i^{t,h}, \xi_i^{t,h}; \mathbf{S}_i^t)$ . Based on the smoothness of  $f^S(\mathbf{X})$ ,  
1449 i.e., Proposition J.5, we have

$$1451 \mathbb{E}[f^S(\mathbf{X}^{t+1})] \leq \mathbb{E}[f^S(\mathbf{X}^t)] - \underbrace{\mathbb{E} \left\langle \nabla_{\mathbf{X}} f^S(\mathbf{X}^t), \gamma \frac{1}{N} \sum_{i=1}^N \sum_{h=0}^{H-1} \mathbf{g}_i^{t,h} \right\rangle}_{T_1} + \frac{\gamma^2 \bar{L}}{2} \mathbb{E} \left\| \frac{1}{N} \sum_{i=1}^N \sum_{h=0}^{H-1} \mathbf{g}_i^{t,h} \right\|^2, \quad (36)$$

1457 where  $\bar{L} = \left(\frac{1}{N} \sum_{i=1}^N \frac{r}{k_i}\right) L$ .

1458 For  $T_1$ , we have  
 1459

$$\begin{aligned}
 1460 \quad T_1 &= -H\mathbb{E} \left\langle \nabla_{\mathbf{X}} f^S(\mathbf{X}^t), \gamma \frac{1}{NH} \sum_{i=1}^N \sum_{h=0}^{H-1} \mathbf{g}_i^{t,h} \right\rangle \\
 1461 &= -H\mathbb{E} \left\langle \nabla_{\mathbf{X}} f^S(\mathbf{X}^t), \gamma \frac{1}{NH} \sum_{i=1}^N \sum_{h=0}^{H-1} \nabla_{\mathbf{X}} f_i^S(\mathbf{X}_i^{t,h}) \right\rangle \\
 1462 &= -\frac{\gamma H}{2} \mathbb{E} \|\nabla_{\mathbf{X}} f^S(\mathbf{X}^t)\|^2 - \frac{\gamma H}{2} \mathbb{E} \left\| \frac{1}{NH} \sum_{i=1}^N \sum_{h=0}^{H-1} \nabla_{\mathbf{X}} f_i^S(\mathbf{X}_i^{t,h}) \right\|^2 \\
 1463 &\quad + \frac{\gamma H}{2} \mathbb{E} \left\| \nabla_{\mathbf{X}} f^S(\mathbf{X}^t) - \frac{1}{NH} \sum_{i=1}^N \sum_{h=0}^{H-1} \nabla_{\mathbf{X}} f_i^S(\mathbf{X}_i^{t,h}) \right\|^2 \\
 1464 &\leq -\frac{\gamma H}{2} \mathbb{E} \|\nabla_{\mathbf{X}} f^S(\mathbf{X}^t)\|^2 - \frac{\gamma H}{2} \mathbb{E} \left\| \frac{1}{N} \sum_{i=1}^N \sum_{h=0}^{H-1} \nabla_{\mathbf{X}} f_i^S(\mathbf{X}_i^{t,h}) \right\|^2 \\
 1465 &\quad + \frac{\gamma}{2} \sum_{h=0}^{H-1} \mathbb{E} \left\| \frac{1}{N} \sum_{i=1}^N \nabla_{\mathbf{X}} f_i^S(\mathbf{X}^t) - \frac{1}{N} \sum_{i=1}^N \nabla_{\mathbf{X}} f_i^S(\mathbf{X}_i^{t,h}) \right\|^2 \\
 1466 &\leq -\frac{\gamma H}{2} \mathbb{E} \|\nabla_{\mathbf{X}} f^S(\mathbf{X}^t)\|^2 - \frac{\gamma}{2H} \mathbb{E} \left\| \frac{1}{N} \sum_{i=1}^N \sum_{h=0}^{H-1} \nabla_{\mathbf{X}} f_i^S(\mathbf{X}_i^{t,h}) \right\|^2 \\
 1467 &\quad + \frac{\gamma H L^2}{2} \frac{1}{NH} \sum_{i=1}^N \frac{r^2}{k_i^2} \sum_{h=0}^{H-1} \mathbb{E} \left\| \mathbf{X}_i^{t,h} - \mathbf{X}^t \right\|^2, \tag{37}
 1468 \\
 1469 &\quad \dots
 1470 \\
 1471 &\quad \dots
 1472 \\
 1473 &\quad \dots
 1474 \\
 1475 &\quad \dots
 1476 \\
 1477 &\quad \dots
 1478 \\
 1479 &\quad \dots
 1480 \\
 1481 &\quad \dots
 1482 \\
 1483 &\quad \dots
 1484
 \end{aligned}$$

1485 where the last inequalities follow Jensen's inequality and Proposition J.5.

1486 For  $T_2$ , we have  
 1487

$$\begin{aligned}
 1488 \quad T_2 &= \mathbb{E} \left\| \frac{1}{N} \sum_{i=1}^N \sum_{h=0}^{H-1} (\mathbf{g}_i^{t,h} \mp \nabla_{\mathbf{X}} f_i^S(\mathbf{X}_i^{t,h})) \right\|^2 \\
 1489 &\leq \frac{2}{N^2} \sum_{i=1}^N \mathbb{E} \left\| \sum_{h=0}^{H-1} (\mathbf{g}_i^{t,h} - \nabla_{\mathbf{X}} f_i^S(\mathbf{X}_i^{t,h})) \right\|^2 + 2\mathbb{E} \left\| \frac{1}{N} \sum_{i=1}^N \sum_{h=0}^{H-1} \nabla_{\mathbf{X}} f_i^S(\mathbf{X}_i^{t,h}) \right\|^2, \tag{38}
 1490 \\
 1491 &\quad \dots
 1492 \\
 1493 &\quad \dots
 1494
 \end{aligned}$$

1495 where the inequality follows the fact that  $\mathbb{E}[\sum_{h=0}^{H-1} (\mathbf{g}_i^{t,h} - \nabla_{\mathbf{X}} f_i^S(\mathbf{X}_i^{t,h}))] = 0$  and the independence  
 1496 between clients.

1497 Furthermore, we bound the first term on the right-hand side of the above inequality as  
 1498

$$\mathbb{E} \left\| \sum_{h=0}^{H-1} (\mathbf{g}_i^{t,h} - \nabla_{\mathbf{X}} f_i^S(\mathbf{X}_i^{t,h})) \right\|^2 = \sum_{h=0}^{H-1} \mathbb{E} \left\| \mathbf{g}_i^{t,h} - \nabla_{\mathbf{X}} f_i^S(\mathbf{X}_i^{t,h}) \right\|^2 \leq H\sigma^2 + \rho \sum_{h=0}^{H-1} \mathbb{E} \left\| \nabla_{\mathbf{X}} f_i^S(\mathbf{X}_i^{t,h}) \right\|^2,$$

1499 where the equality follows Lemma J.2 and the inequality follows Assumption 4.2. For  
 1500  $\left\| \nabla_{\mathbf{X}} f_i^S(\mathbf{X}_i^{t,h}) \right\|^2$ , utilizing Assumption 4.3 and Proposition J.5, we have  
 1501

$$\begin{aligned}
 1502 \quad &\left\| \nabla_{\mathbf{X}} f_i^S(\mathbf{X}_i^{t,h}) \right\|^2 = \left\| \nabla_{\mathbf{X}} f_i^S(\mathbf{X}_i^{t,h}) \mp \nabla_{\mathbf{X}} f_i^S(\mathbf{X}^t) \mp \nabla_{\mathbf{X}} f^S(\mathbf{X}^t) \right\|^2 \\
 1503 &\leq 3 \left\| \nabla_{\mathbf{X}} f_i^S(\mathbf{X}_i^{t,h}) - \nabla_{\mathbf{X}} f_i^S(\mathbf{X}^t) \right\|^2 + 3 \left\| \nabla_{\mathbf{X}} f_i^S(\mathbf{X}^t) - \nabla_{\mathbf{X}} f^S(\mathbf{X}^t) \right\|^2 + 3 \left\| \nabla_{\mathbf{X}} f^S(\mathbf{X}^t) \right\|^2 \\
 1504 &\leq 3 \frac{r^2}{k_i^2} L^2 \left\| \mathbf{X}_i^{t,h} - \mathbf{X}^t \right\|^2 + 3(c_h + 1) \|\nabla_{\mathbf{X}} f^S(\mathbf{X}^t)\|^2 + 3\rho\delta_h^2. \tag{39}
 1505 \\
 1506 &\quad \dots
 1507 \\
 1508 &\quad \dots
 1509 \\
 1510 &\quad \dots
 1511
 \end{aligned}$$

Combining the above three inequalities gives rise to

$$T_2 \leq \frac{2H}{N}(\sigma^2 + 3\rho\delta_h^2) + 2\mathbb{E} \left\| \frac{1}{N} \sum_{i=1}^N \sum_{h=0}^{H-1} \nabla_{\mathbf{X}} f_i^S(\mathbf{X}_i^{t,h}) \right\|^2 + \frac{6\rho(c_h + 1)H}{N} \mathbb{E} \|\nabla_{\mathbf{X}} f^S(\mathbf{X}^t)\|^2 + \frac{6\rho HL^2}{N} T_3, \quad (40)$$

where  $T_3 = \frac{1}{NH} \sum_{i=1}^N \frac{r^2}{k_i^2} \sum_{h=0}^{H-1} \mathbb{E} \left\| \mathbf{X}_i^{t,h} - \mathbf{X}^t \right\|^2$ . Combining (36), (37), and (40) yields

$$\begin{aligned} \mathbb{E}[f^S(\mathbf{X}^{t+1})] &\leq \mathbb{E}[f^S(\mathbf{X}^t)] - \left( \frac{\gamma H}{2} - 3\gamma^2 \rho(c_h + 1) \frac{H}{N} \bar{L} \right) \mathbb{E} \|\nabla_{\mathbf{X}} f^S(\mathbf{X}^t)\|^2 + \gamma^2 \bar{L} \frac{H}{N} (\sigma^2 + 3\rho\sigma_h^2) \\ &\quad - \left( \frac{\gamma}{2H} - \gamma^2 \bar{L} \right) \mathbb{E} \left\| \frac{1}{N} \sum_{i=1}^N \sum_{h=0}^{H-1} \nabla_{\mathbf{X}} f_i^S(\mathbf{X}_i^{t,h}) \right\|^2 + \left( \frac{\gamma HL^2}{2} + 3\gamma^2 \rho \bar{L} L^2 \frac{H}{N} \right) T_3, \end{aligned} \quad (41)$$

where  $\bar{L} = \left( \frac{1}{N} \sum_{i=1}^N \frac{r}{k_i} \right) L$ . Let  $\gamma \leq \min\{\frac{N}{24\rho(c_h+1)H\bar{L}}, \frac{1}{2H\bar{L}}, \frac{N}{6\rho\bar{L}}\}$ , we have

$$\mathbb{E}[f^S(\mathbf{X}^{t+1})] \leq \mathbb{E}[f^S(\mathbf{X}^t)] - \frac{3\gamma H}{8} \mathbb{E} \|\nabla_{\mathbf{X}} f^S(\mathbf{X}^t)\|^2 + \gamma^2 \bar{L} \frac{H}{N} (\sigma^2 + 3\rho\sigma_h^2) + \frac{5\gamma}{8} HL^2 T_3. \quad (42)$$

For  $T_3$ , we have

$$\begin{aligned} T_3 &= \frac{1}{NH} \sum_{i=1}^N \frac{r^2}{k_i^2} \sum_{h=0}^{H-1} \mathbb{E} \left\| \gamma \sum_{\tau=0}^{h-1} \mathbf{g}_i^{t,\tau} \right\|^2 \\ &= \gamma^2 \frac{1}{NH} \sum_{i=1}^N \frac{r^2}{k_i^2} \sum_{h=0}^{H-1} \mathbb{E} \left\| \sum_{\tau=0}^{h-1} (\mathbf{g}_i^{t,\tau} \mp \nabla_{\mathbf{X}} f_i^S(\mathbf{X}_i^{t,\tau})) \right\|^2 \\ &\leq 2\gamma^2 \frac{1}{NH} \sum_{i=1}^N \frac{r^2}{k_i^2} \sum_{h=0}^{H-1} \sum_{\tau=0}^{h-1} \mathbb{E} \|\mathbf{g}_i^{t,\tau} - \nabla_{\mathbf{X}} f_i^S(\mathbf{X}_i^{t,\tau})\|^2 + 2\gamma^2 \frac{1}{NH} \sum_{i=1}^N \frac{r^2}{k_i^2} \sum_{h=0}^{H-1} h \sum_{\tau=0}^{h-1} \mathbb{E} \|\nabla_{\mathbf{X}} f_i^S(\mathbf{X}_i^{t,\tau})\|^2 \\ &\leq 2\gamma^2 H \sigma^2 \left( \frac{1}{N} \sum_{i=1}^N \frac{r^2}{k_i^2} \right) + \frac{2\rho\gamma^2}{NH} \sum_{i=1}^N \frac{r^2}{k_i^2} \sum_{h=0}^{H-1} \sum_{\tau=0}^{h-1} \mathbb{E} \|\nabla_{\mathbf{X}} f_i^S(\mathbf{X}_i^{t,\tau})\|^2 \\ &\quad + \frac{2\gamma^2}{NH} \sum_{i=1}^N \frac{r^2}{k_i^2} \sum_{h=0}^{H-1} h \sum_{\tau=0}^{h-1} \mathbb{E} \|\nabla_{\mathbf{X}} f_i^S(\mathbf{X}_i^{t,\tau})\|^2 \\ &\leq 2\gamma^2 H \sigma^2 \left( \frac{1}{N} \sum_{i=1}^N \frac{r^2}{k_i^2} \right) + \frac{2(\rho+1)\gamma^2 H}{N} \sum_{i=1}^N \frac{r^2}{k_i^2} \sum_{h=0}^{H-1} \mathbb{E} \|\nabla_{\mathbf{X}} f_i^S(\mathbf{X}_i^{t,\tau})\|^2. \end{aligned} \quad (43)$$

Plugging inequality (39) into inequality (43) yeilds

$$\begin{aligned} T_3 &\leq 2\gamma^2 H \left( \frac{1}{N} \sum_{i=1}^N \frac{r^2}{k_i^2} \right) \sigma^2 + 6(\rho+1)\gamma^2 H^2 \left( \frac{1}{N} \sum_{i=1}^N \frac{r^2}{k_i^2} \right) \sigma_h^2 \\ &\quad + 6(\rho+1)\gamma^2 L^2 H^2 T_3 + 6(\rho+1) \left( \frac{1}{N} \sum_{i=1}^N \frac{r^2}{k_i^2} \right) (c_h + 1) \gamma^2 H^2 \mathbb{E} \|\nabla_{\mathbf{X}} f^S(\mathbf{X}^t)\|^2. \end{aligned} \quad (44)$$

Denote  $\kappa = \frac{1}{N} \sum_{i=1}^N \frac{r^2}{k_i^2}$ , we simplify the above inequality as

$$(1 - 6(\rho+1)\gamma^2 L^2 H^2) T_3 \leq 2\kappa\gamma^2 H^2 (\sigma_g^2 + 3(\rho+1)\sigma_h^2) + 6\kappa(\rho+1)(c_h + 1) \gamma^2 H^2 \mathbb{E} \|\nabla_{\mathbf{X}} f^S(\mathbf{X}^t)\|^2.$$

Let  $\gamma \leq \frac{1}{\sqrt{12(\rho+1)HL}}$ , we get the bound for  $T_3$

$$T_3 \leq 4\kappa\gamma^2 H^2 (\sigma^2 + 3(\rho+1)\sigma_h^2) + 12\kappa(\rho+1)(c_h + 1) \gamma^2 H^2 \mathbb{E} \|\nabla_{\mathbf{X}} f^S(\mathbf{X}^t)\|^2. \quad (45)$$

1566 Plugging the bound for  $T_3$  into inequality (42) gives rise to  
 1567

$$\begin{aligned} 1568 \mathbb{E}[f^S(\mathbf{X}^{t+1})] &\leq \mathbb{E}[f^S(\mathbf{X}^t)] - \left(\frac{3\gamma H}{8} - \frac{5\gamma H}{8}L^2(12\kappa(\rho+1)(c_h+1)\gamma^2 H^2)\right)\mathbb{E}\|\nabla_{\mathbf{X}}f^S(\mathbf{X}^t)\|^2 \\ 1569 \\ 1570 &\quad + \gamma^2\bar{L}\frac{H}{N}(\sigma^2 + 3\rho\sigma_h^2) + \frac{5\gamma}{8}HL^2 \cdot 4\kappa\gamma^2H^2(\sigma^2 + 3(\rho+1)\sigma_h^2). \end{aligned} \quad (46)$$

1571 Let  $\gamma \leq \frac{1}{8\sqrt{\kappa(\rho+1)(c_h+1)HL}}$ , we obtain  
 1572

$$\mathbb{E}[f^S(\mathbf{X}^{t+1})] \leq \mathbb{E}[f^S(\mathbf{X}^t)] - \frac{\gamma H}{4}\mathbb{E}\|\nabla_{\mathbf{X}}f^S(\mathbf{X}^t)\|^2 + \gamma^2\bar{L}\frac{H}{N}\sigma_\rho^2 + \frac{5}{2}\kappa\gamma^3H^3L^2\sigma_\rho^2, \quad (47)$$

1573 where  $\sigma_\rho^2 = \sigma^2 + 3(\rho+1)\sigma_h^2$ .  
 1574

1575 Telescoping the above inequality from  $t = 0$  to  $T - 1$ , we have  
 1576

$$\frac{1}{T}\sum_{t=0}^{T-1}\mathbb{E}\|\nabla_{\mathbf{X}}f^S(\mathbf{X}^t)\|^2 \leq 4\frac{f^S(\mathbf{X}^0) - f^*}{\gamma TH} + \gamma\frac{4\bar{L}}{N}\sigma_\rho^2 + 10\gamma^2H^2\tilde{L}L\sigma_\rho^2, \quad (48)$$

1577 where  $f^*$  denotes the lower bound of  $f^S(\mathbf{X})$  and  $\tilde{L} = \kappa L$ .  
 1578

1579 Applying Lemma J.3 to the above inequality and letting  $d = H$ , it follows that there exists a learning  
 1580 rate  $\gamma \leq \min\{\frac{N}{24\rho(c_h+1)H\bar{L}}, \frac{1}{8\sqrt{\tilde{L}L(\rho+1)(c_h+1)H}}, \frac{1}{H}\}$  such that  
 1581

$$\frac{1}{T}\sum_{t=0}^{T-1}\mathbb{E}\|\nabla_{\mathbf{X}}f^S(\mathbf{X}^t)\|^2 \leq 8\frac{\sqrt{\bar{L}\mathcal{F}_0\sigma_\rho^2}}{\sqrt{NTH}} + 10(\tilde{L}L)^{\frac{1}{3}}\left(\frac{\mathcal{F}_0\sigma_\rho}{T}\right)^{\frac{2}{3}} + \frac{4\mathcal{F}_0}{T}. \quad (49)$$

1582 This completes the proof of Theorem 4.4.  
 1583

#### 1584 J.4 PROOF OF PROPOSITION J.5

1585 i) For illustration, we need to recover  $\mathbf{X}$  to  $[\mathbf{B}; \mathbf{A}]$  in this proof. According to the definition of  
 1586  $\tilde{f}_i(\mathbf{X}; \mathbf{S})$  and  $f_i(\mathbf{B}, \mathbf{A})$ , we have  
 1587

$$\tilde{f}_i(\mathbf{X}; \mathbf{S}) = \tilde{f}_i(\mathbf{B}, \mathbf{A}; \mathbf{S}) \quad (50)$$

$$\begin{aligned} 1588 \\ 1589 &= \mathbb{E}_{\xi \sim \mathcal{D}_i} [\ell(\mathbf{W}_0 + \mathbf{BS}\mathbf{A}, \xi)] \\ 1590 \\ 1591 &= f_i(\mathbf{BS}, \mathbf{A}). \end{aligned} \quad (51)$$

1592 As  $f_i(\mathbf{B}, \mathbf{A})$  is  $L$ -smooth, we have  
 1593

$$f_i(\mathbf{BS} + \Delta\mathbf{BS}, \mathbf{A} + \Delta\mathbf{A}) \leq f_i(\mathbf{BS}, \mathbf{A}) + \left\langle \begin{bmatrix} \nabla_{\mathbf{BS}}f_i(\mathbf{BS}, \mathbf{A}) \\ \nabla_{\mathbf{A}}f_i(\mathbf{BS}, \mathbf{A}) \end{bmatrix}, \begin{bmatrix} \Delta\mathbf{BS} \\ \Delta\mathbf{A} \end{bmatrix} \right\rangle + \frac{L}{2} \left\| \begin{bmatrix} \Delta\mathbf{BS} \\ \Delta\mathbf{A} \end{bmatrix} \right\|^2. \quad (52)$$

1594 According to (50) and (51), we have  $\tilde{f}_i(\mathbf{B} + \Delta\mathbf{B}, \mathbf{A} + \Delta\mathbf{A}; \mathbf{S}) = f_i(\mathbf{BS} + \Delta\mathbf{BS}, \mathbf{A} + \Delta\mathbf{A})$  and  
 1595  $\tilde{f}_i(\mathbf{B}, \mathbf{A}; \mathbf{S}) = f_i(\mathbf{BS}, \mathbf{A})$ . Combining these with (52) gives rise to  
 1596

$$\tilde{f}_i(\mathbf{B} + \Delta\mathbf{B}, \mathbf{A} + \Delta\mathbf{A}; \mathbf{S}) \leq \tilde{f}_i(\mathbf{B}, \mathbf{A}; \mathbf{S}) + \left\langle \begin{bmatrix} \nabla_{\mathbf{BS}}f_i(\mathbf{BS}, \mathbf{A}) \\ \nabla_{\mathbf{A}}f_i(\mathbf{BS}, \mathbf{A}) \end{bmatrix}, \begin{bmatrix} \Delta\mathbf{BS} \\ \Delta\mathbf{A} \end{bmatrix} \right\rangle + \frac{L}{2} \left\| \begin{bmatrix} \Delta\mathbf{BS} \\ \Delta\mathbf{A} \end{bmatrix} \right\|^2. \quad (53)$$

1597 We denote  
 1598

$$L(\mathbf{W}_0 + \mathbf{BS}\mathbf{A}) = \tilde{f}_i(\mathbf{B}, \mathbf{A}; \mathbf{S}) = \mathbb{E}_{\xi \sim \mathcal{D}_i} [\ell(\mathbf{W}_0 + \mathbf{BS}\mathbf{A}, \xi)]. \quad (54)$$

1599 Note that  $\nabla_{\mathbf{BS}}f_i(\mathbf{BS}, \mathbf{A}) = \nabla L(\mathbf{W}_0 + \mathbf{BS}\mathbf{A})\mathbf{A}^\top$  and  $\nabla_{\mathbf{A}}f_i(\mathbf{BS}, \mathbf{A}) = \mathbf{S}^\top\mathbf{B}^\top\nabla L(\mathbf{W}_0 + \mathbf{BS}\mathbf{A})$ .  
 1600 We thus have  
 1601

$$\begin{aligned} 1602 \\ 1603 &\left\langle \begin{bmatrix} \nabla_{\mathbf{BS}}f_i(\mathbf{BS}, \mathbf{A}) \\ \nabla_{\mathbf{A}}f_i(\mathbf{BS}, \mathbf{A}) \end{bmatrix}, \begin{bmatrix} \Delta\mathbf{BS} \\ \Delta\mathbf{A} \end{bmatrix} \right\rangle = \left\langle \begin{bmatrix} \nabla L(\mathbf{W}_0 + \mathbf{BS}\mathbf{A})\mathbf{A}^\top \\ \mathbf{S}^\top\mathbf{B}^\top\nabla L(\mathbf{W}_0 + \mathbf{BS}\mathbf{A}) \end{bmatrix}, \begin{bmatrix} \Delta\mathbf{BS} \\ \Delta\mathbf{A} \end{bmatrix} \right\rangle \\ 1604 \\ 1605 &= \left\langle \begin{bmatrix} \nabla L(\mathbf{W}_0 + \mathbf{BS}\mathbf{A})\mathbf{A}^\top\mathbf{S}^\top \\ \mathbf{S}^\top\mathbf{B}^\top\nabla L(\mathbf{W}_0 + \mathbf{BS}\mathbf{A}) \end{bmatrix}, \begin{bmatrix} \Delta\mathbf{B} \\ \Delta\mathbf{A} \end{bmatrix} \right\rangle \\ 1606 \\ 1607 &= \left\langle \begin{bmatrix} \nabla_{\mathbf{B}}\tilde{f}_i(\mathbf{B}, \mathbf{A}; \mathbf{S}) \\ \nabla_{\mathbf{A}}\tilde{f}_i(\mathbf{B}, \mathbf{A}; \mathbf{S}) \end{bmatrix}, \begin{bmatrix} \Delta\mathbf{B} \\ \Delta\mathbf{A} \end{bmatrix} \right\rangle, \end{aligned} \quad (55)$$

1620 where the last equality follows the fact that  $\tilde{f}_i(\mathbf{B}, \mathbf{A}; \mathbf{S}) = L(\mathbf{W}_0 + \mathbf{BSA})$  defined in (54) and  
 1621

$$1622 \begin{bmatrix} \nabla_{\mathbf{B}} \tilde{f}_i(\mathbf{B}, \mathbf{A}; \mathbf{S}) \\ \nabla_{\mathbf{A}} \tilde{f}_i(\mathbf{B}, \mathbf{A}; \mathbf{S}) \end{bmatrix} = \begin{bmatrix} \nabla L(\mathbf{W}_0 + \mathbf{BSA}) \mathbf{A}^\top \mathbf{S}^\top \\ \mathbf{S}^\top \mathbf{B}^\top \nabla L(\mathbf{W}_0 + \mathbf{BSA}) \end{bmatrix}. \quad (56)$$

1624 Plugging (55) into (53) gives rise to  
 1625

$$1626 \tilde{f}_i(\mathbf{B} + \Delta \mathbf{B}, \mathbf{A} + \Delta \mathbf{A}; \mathbf{S}) \leq \tilde{f}_i(\mathbf{B}, \mathbf{A}; \mathbf{S}) + \left\langle \begin{bmatrix} \nabla_{\mathbf{B}} \tilde{f}_i(\mathbf{B}, \mathbf{A}; \mathbf{S}) \\ \nabla_{\mathbf{A}} \tilde{f}_i(\mathbf{B}, \mathbf{A}; \mathbf{S}) \end{bmatrix}, \begin{bmatrix} \Delta \mathbf{B} \\ \Delta \mathbf{A} \end{bmatrix} \right\rangle + \frac{L}{2} \left\| \begin{bmatrix} \Delta \mathbf{B} \\ \Delta \mathbf{A} \end{bmatrix} \right\|^2. \quad (57)$$

1630 In particular,  $\left\| \begin{bmatrix} \Delta \mathbf{B} \\ \Delta \mathbf{A} \end{bmatrix} \right\|^2 = \|\Delta \mathbf{B}\|^2 + \|\Delta \mathbf{A}\|^2$ . From (24), we know  $\|\Delta \mathbf{B}\|^2 \leq \frac{r^2}{k_i^2} \|\Delta \mathbf{B}\|^2$ .  
 1631

1632 Therefore, we have  $\left\| \begin{bmatrix} \Delta \mathbf{B} \\ \Delta \mathbf{A} \end{bmatrix} \right\|^2 = \frac{r^2}{k_i^2} \left\| \begin{bmatrix} \Delta \mathbf{B} \\ \Delta \mathbf{A} \end{bmatrix} \right\|^2$ . As a result,  $\tilde{f}_i(\mathbf{B}, \mathbf{A}; \mathbf{S})$  (i.e.,  $\tilde{f}_i(\mathbf{X}, \mathbf{S})$ ) is  $L \frac{r^2}{k_i^2}$ -smooth.  
 1633

1634 ii) Note that  $f_i^S(\mathbf{X}) = \mathbb{E}_{\mathbf{S} \sim \mathcal{S}_i} [\tilde{f}_i(\mathbf{X}, \mathbf{S})]$ . Therefore, we further take expectation for (57) over  $\mathbf{S} \sim \mathcal{S}_i$ ,  
 1635 leading to  
 1636

$$1637 f_i^S(\mathbf{B} + \Delta \mathbf{B}, \mathbf{A} + \Delta \mathbf{A}) \leq f_i^S(\mathbf{B}, \mathbf{A}) + \left\langle \begin{bmatrix} \nabla_{\mathbf{B}} f_i^S(\mathbf{B}, \mathbf{A}) \\ \nabla_{\mathbf{A}} f_i^S(\mathbf{B}, \mathbf{A}) \end{bmatrix}, \begin{bmatrix} \Delta \mathbf{B} \\ \Delta \mathbf{A} \end{bmatrix} \right\rangle + \frac{L}{2} \mathbb{E}_{\mathbf{S} \sim \mathcal{S}_i} \left\| \begin{bmatrix} \Delta \mathbf{B} \\ \Delta \mathbf{A} \end{bmatrix} \right\|^2. \quad (58)$$

1638 In particular,  $\mathbb{E}_{\mathbf{S} \sim \mathcal{S}_i} \left\| \begin{bmatrix} \Delta \mathbf{B} \\ \Delta \mathbf{A} \end{bmatrix} \right\|^2 = \mathbb{E}_{\mathbf{S} \sim \mathcal{S}_i} \|\Delta \mathbf{B}\|^2 + \|\Delta \mathbf{A}\|^2$ . From (25), we know  
 1639

1640  $\mathbb{E}_{\mathbf{S} \sim \mathcal{S}_i} \|\Delta \mathbf{B}\|^2 \leq \frac{r}{k_i} \|\Delta \mathbf{B}\|^2$ . In other words,  $\mathbb{E}_{\mathbf{S} \sim \mathcal{S}_i} \left\| \begin{bmatrix} \Delta \mathbf{B} \\ \Delta \mathbf{A} \end{bmatrix} \right\|^2 \leq \frac{r}{k_i} \left\| \begin{bmatrix} \Delta \mathbf{B} \\ \Delta \mathbf{A} \end{bmatrix} \right\|^2$ . We thus claim  
 1641 that  $f_i^S(\mathbf{B}, \mathbf{A})$  (i.e.,  $f_i^S(\mathbf{X})$ ) is  $L \frac{r}{k_i}$ -smooth.  
 1642

1643 iii) Finally, for  $f^S(\mathbf{X}) = \frac{1}{N} \sum_{i=1}^N f_i^S(\mathbf{X})$ , we have  
 1644

$$1645 \nabla f^S(\mathbf{X}) = \frac{1}{N} \sum_{i=1}^N \nabla f_i^S(\mathbf{X}). \quad (59)$$

1646 Since  $f_i^S(\mathbf{X})$  is  $L \frac{r}{k_i}$ -smooth, we thus have  
 1647

$$1648 \|\nabla f_i^S(\mathbf{X}) - \nabla f_i^S(\mathbf{Y})\| \leq L \frac{r}{k_i} \|\mathbf{X} - \mathbf{Y}\|, \quad \forall \mathbf{X}, \mathbf{Y}. \quad (60)$$

1649 To find the Lipschitz constant of  $f^S(\mathbf{X})$ , we analyze the difference between the gradients at two  
 1650 points  $\mathbf{X}$  and  $\mathbf{Y}$ :  
 1651

$$1652 \begin{aligned} \|\nabla f^S(\mathbf{X}) - \nabla f^S(\mathbf{Y})\| &= \left\| \frac{1}{N} \sum_{i=1}^N (\nabla f_i^S(\mathbf{X}) - \nabla f_i^S(\mathbf{Y})) \right\| \\ 1653 &\leq \frac{1}{N} \sum_{i=1}^N \|\nabla f_i^S(\mathbf{X}) - \nabla f_i^S(\mathbf{Y})\| \\ 1654 &\leq \left( \frac{1}{N} \sum_{i=1}^N \frac{r}{k_i} L \right) \|\mathbf{X} - \mathbf{Y}\|. \end{aligned} \quad (61)$$

1655 Therefore,  $f^S(\mathbf{X})$  is  $\left( \frac{1}{N} \sum_{i=1}^N \frac{r}{k_i} L \right)$ -smooth.  
 1656

1657  
 1658  
 1659  
 1660  
 1661  
 1662  
 1663  
 1664  
 1665  
 1666  
 1667  
 1668  
 1669  
 1670  
 1671  
 1672  
 1673